

# Chapter 5. Brief history of climate: causes and mechanisms

## 5.1 Introduction

Since the beginning of Earth's history, climate has varied on all timescales. Over millions of years, it has swung between very warm conditions, with annual mean temperatures above 10°C in polar regions and glacial climates in which the ice sheets covered the majority of the mid-latitude continents. It has even been postulated that, in some past cold periods, the whole surface of the Earth was covered by ice (this is the snowball Earth hypothesis). At the other end of the spectrum, lower amplitude fluctuations are observed at interannual and decadal timescales, no year being exactly the same as to a previous one.

The **timescale** of these variations is partly set up by the forcing (Fig. 5.1). Because of its own stellar evolution, the radiation emitted by the Sun has increased by roughly 30% over the 4.5 billion years of the Earth's history. Variations in the **total solar irradiance** on shorter timescales have a smaller amplitude, although this amplitude is not precisely known (see Section 5.5). The low frequency changes of the characteristics of the Earth orbit (see Section 5.4.1) modify the amount of solar energy received in a particular season on every point on the Earth's surface, with the most important fluctuations located in the 10-100 ka range. Individual volcanic eruptions produce a general cooling during the years following the eruption (see Section 5.5.1). Furthermore, volcanic activity can be responsible for low frequency forcing if large eruptions are grouped in a particular decade or century. On longer **timescales**, increased volcanic activity related to plate tectonics can lead to a strong lasting thousands to millions of years.

On the other hand, internal dynamics also play a very important role in determining the variability of the Earth's climate. They can be a direct cause of variability, in the absence of any significant change in the forcing, through interactions between various elements of the system. Important examples are the El Niño Southern Oscillation (ENSO), the North Atlantic Oscillation (NAO) and the Southern Annular Mode (SAM). Secondly, because of the large inertia of the ocean and the ice sheets, the dominant effect of a perturbation can be related to the integration of the forcing over long time scales while higher frequency changes are damped. Inertia can also induce a delayed response to a perturbation (see Section 4.1.3). Furthermore, the response of the system can involve complex mechanisms that lead to large differences between the characteristics of forcing and those of the climate changes induced by the forcing. For instance, if a forcing excites one mode of internal variability of the system at a particular frequency, leading to a kind of resonance, the magnitude of the response at that frequency will be large even though the forcing is not particularly intense at that frequency. Small changes in the forcing can also lead to large variations in the climate system if a threshold is crossed and, as a result the system evolves (nearly-) spontaneously from one state to another, possibly quite different, one. Such a transition, involving the deep oceanic circulation, has been proposed to explain some of the abrupt climate changes recorded in Greenland ice cores during the last glacial period.

This brief overview has described a few of the processes that have to be combined to explain past climate changes. Below, we will illustrate some of the most important concepts, starting with the variability that is due to internal processes only. For this, we will focus on processes characterised by relatively high frequency variations, because

they are the ones for which we have the most information. The components of the climate system that are mainly involved in those modes of variability are the atmosphere and the surface layer of the ocean. The internal variability of the deep ocean circulation and the ice sheets will not be discussed here. We will then review past climate changes, starting with very long timescales and finishing with the last millennium.

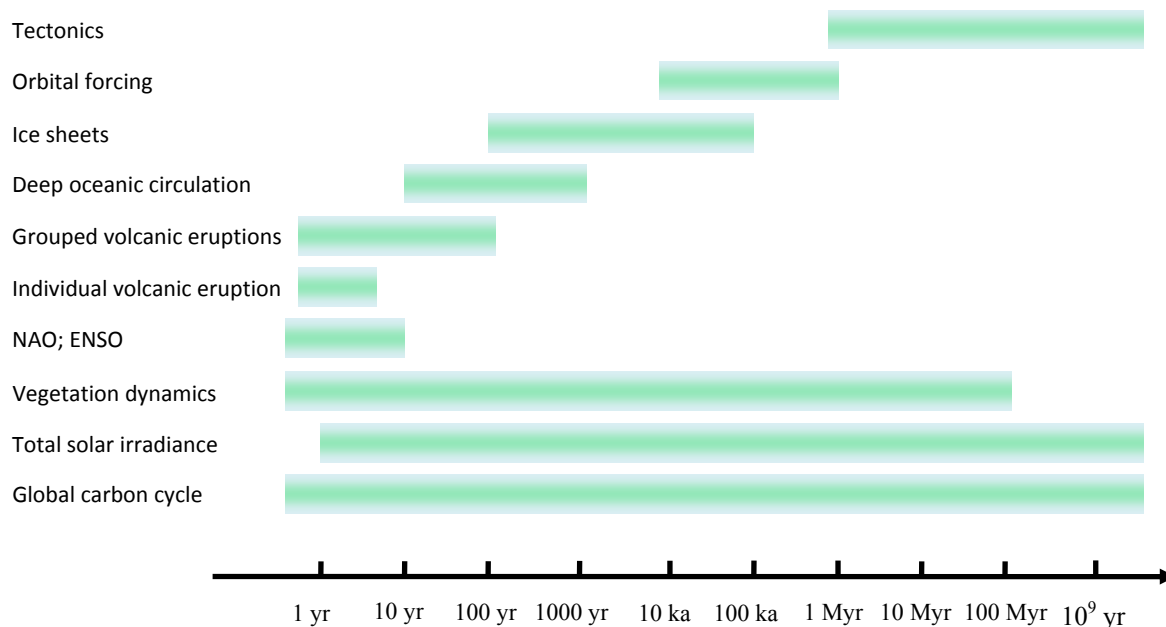


Figure 5.1. Schematic representation of the dominant timescales of some selected external forcing and processes related to internal dynamics that affect climate. For each of them, we have plotted here an indicative range. However, because of mutual interactions, they can exhibit variability on nearly all the timescales. For instance, orbital forcing could influence the distribution of temperature and precipitation at the Earth surface and then induce variations of the oceanic circulation and ENSO on multi-millennial timescales.

## 5.2 Internal climate variability

### 5.2.1 El Niño-Southern Oscillation

In equatorial regions, the **trade winds** induce a **zonal** transport from the East to the West Pacific that is responsible for warm sea surface temperatures and a relatively deep **thermocline** there. The **thermocline** is higher in the East Pacific. As a consequence, the equatorial **upwelling** (also caused by the **trade winds**) transports cold deep water to the surface more efficiently in the East Pacific, leading to a large cooling in this region (see Section 1.3 and Fig. 5.2).

Because of those differences in sea surface temperatures (SSTs), atmospheric convection and **ascendant** air motion are observed over the West Pacific while **subsidence** occurs over the East Pacific. The circulation is closed by an movement transport in the upper troposphere and westward atmospheric flow in the lower layers (Fig. 5.2). The resulting **zonal** overturning circulation, referred to as the **Walker circulation**, thus reinforces the easterlies that are the **zonal** mean in this latitude band

(see Section 1.2). Consequently, the Walker circulation is associated with a positive **feedback**, called the Bjerknes **feedback** (Fig. 5.3), in which the easterly surface wind stress enhances the zonal SST **gradient** which in turns amplifies the wind stress.

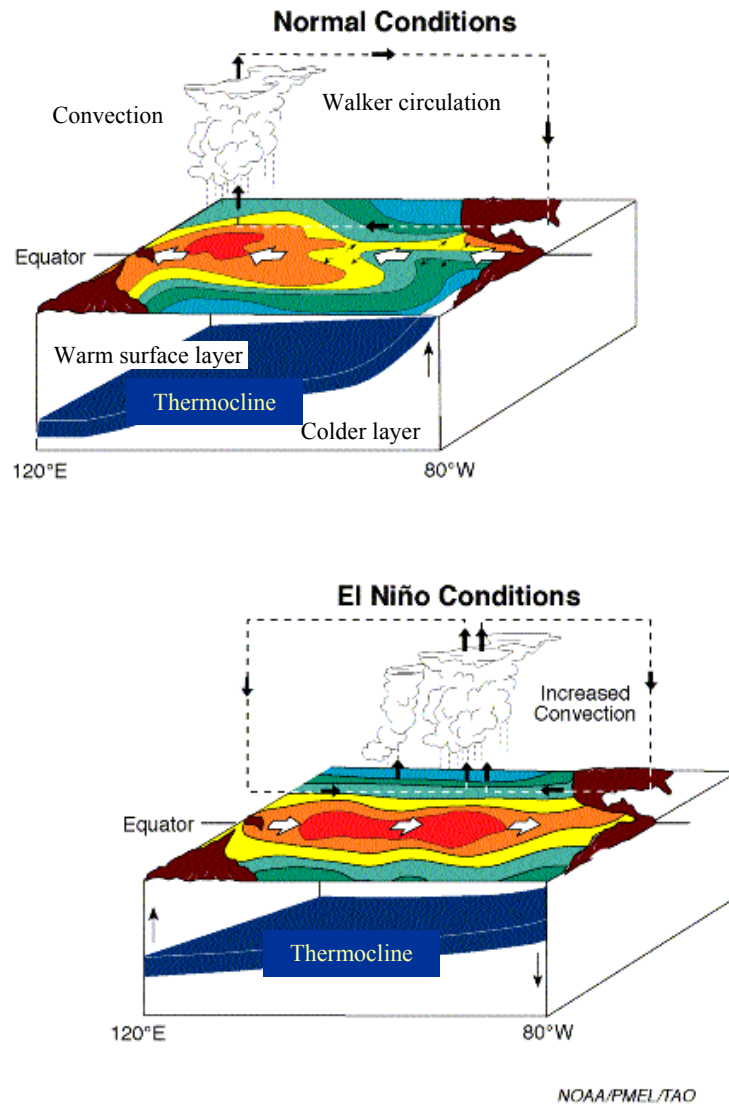


Figure 5.2. The Walker circulation in the atmosphere and the position of the thermocline in the ocean in normal conditions and in El Niño years. Red represents warm SST while green ones represents cold water. *Source:* <http://www.pmel.noaa.gov/tao/elnino/el-nino-story.html>. Following the policy of U.S. government agencies, this figure is not subject to copyright protection.

The Walker circulation exhibits irregular oscillations (Fig.5.4). They are characterised by a see-saw in sea level pressure (SLP) between the East and West Pacific that drives the surface easterlies (Fig. 5.5). Classically, the magnitude of this mode is measured by the Southern Oscillation Index (SOI):

$$SOI = 10 \frac{SLP'_{Tahiti} - SLP'_{Darwin}}{\sigma_{\Delta SLP}} \quad (5.1)$$

where the  $SLP'_{Tahiti}$  and  $SLP'_{Darwin}$  are SLP **anomalies** (i.e. the difference between the current value and the long term mean) at Tahiti and Darwin (Australia), respectively and  $\sigma_{ASLP}$  is the standard deviation of the difference between these two SLP anomalies.

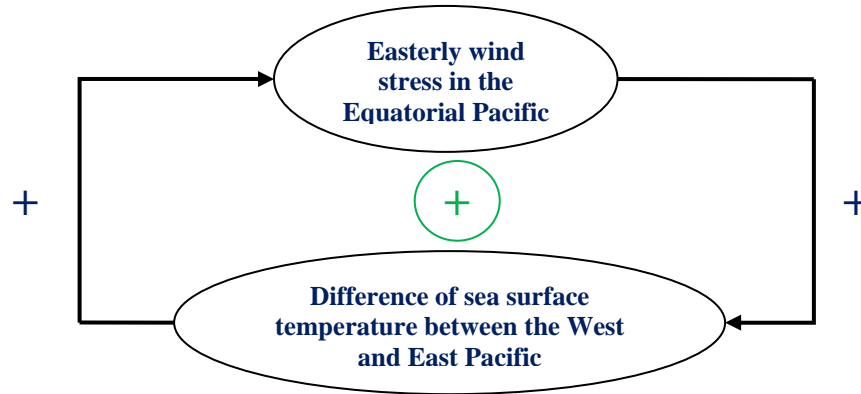


Figure 5.3. Flow graph illustrating the Bjerknes **feedback**. A positive sign on an arrow show that an increase in one variable produces an increase in the other. The positive sign inside a circle indicates that the overall feedback is positive.

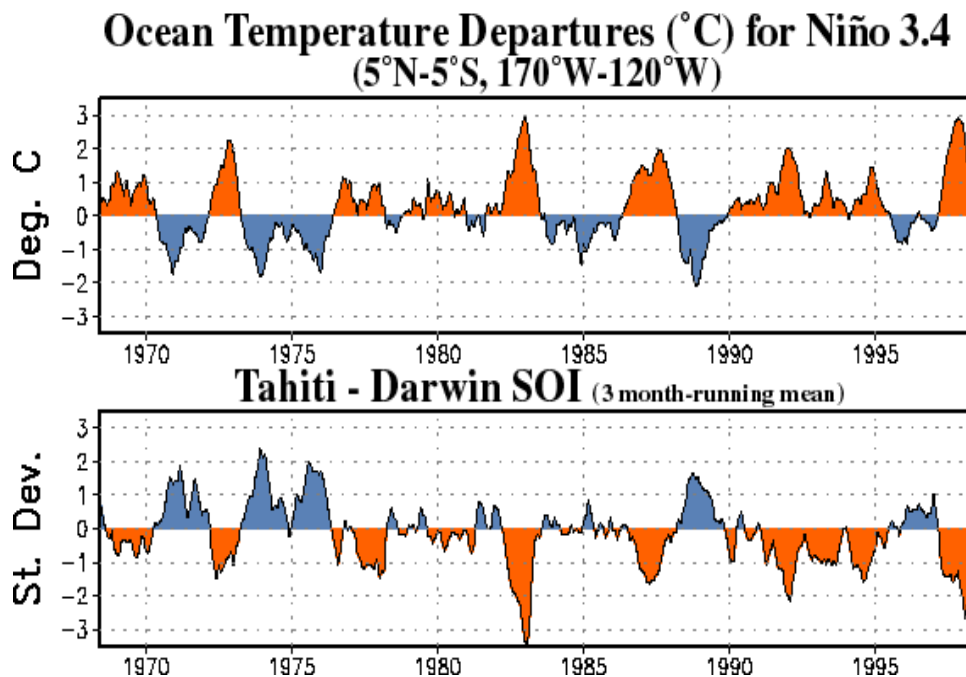


Figure 5.4. Time series of the temperature in the eastern equatorial Pacific (averaged over the area  $5^{\circ}\text{N}-5^{\circ}\text{S}-170^{\circ}\text{W}-120^{\circ}\text{W}$ , the so-called Niño3.4 index) and the SOI index. A filter has been applied to remove fluctuations with periods less than a few months. Negative values of the SOI and positive temperature **anomalies** correspond to El Niño episodes (e.g., the years 1982/83 and 1997/98) while a positive SOI index and a negative temperature **anomaly** in the Eastern Equatorial Pacific are typical of La Niña periods (e.g., the years 1988/89, 1995/96). *Source:* [http://www.cpc.ncep.noaa.gov/products/analysis\\_monitoring/ensocycle/soi.shtml](http://www.cpc.ncep.noaa.gov/products/analysis_monitoring/ensocycle/soi.shtml). Following the policy of U.S. government agencies, this figure is not subject to copyright protection.

When the SOI is low, the long term mean gradient between the East and West Pacific decreases, leading to weaker easterlies. Prolonged negative values of the SOI are thus associated with reduced **upwelling** and weaker westward oceanic currents. This induces a smaller east-west tilt of the **thermocline** and abnormally warm surface temperatures in the East Equatorial Pacific (Figs. 5.2 and 5.4). The temperature **anomaly** can reach 5°C locally. The associated warming close to the coast of Peru was originally referred to as El Niño, but the term is now used to describe all the oceanic changes that occur when temperature is high in the East Pacific Ocean. The opposite condition, corresponding to colder temperatures in the East Pacific, an increased tilt in the ocean **thermocline**, and warm surface water restricted to the West Pacific are called, by analogy, La Niña conditions.

Because of the strong interactions between oceanic and atmospheric changes, the Southern Oscillation and the El Niño phenomenon are strongly coupled (see Fig. 5.4). This has led to the choice of the acronym ENSO (El Niño Southern Oscillation) to refer to the whole process. Indeed, because of the Bjerknes **feedback**, a decrease in **zonal** SST gradient, caused for instance by a relaxation of the tilt of the **thermocline**, implies a reduction of the **zonal** wind stress that will amplify the initial perturbation. The anomalies then grow until negative feedbacks, mainly related to oceanic processes (in particular the adjustment of the **thermocline** depth) overwhelm the positive feedbacks. Those negative feedbacks are characterised by a delayed response compared to the SST and wind stress initial perturbation, allowing the development of the irregular oscillation described in Fig. 5.4.

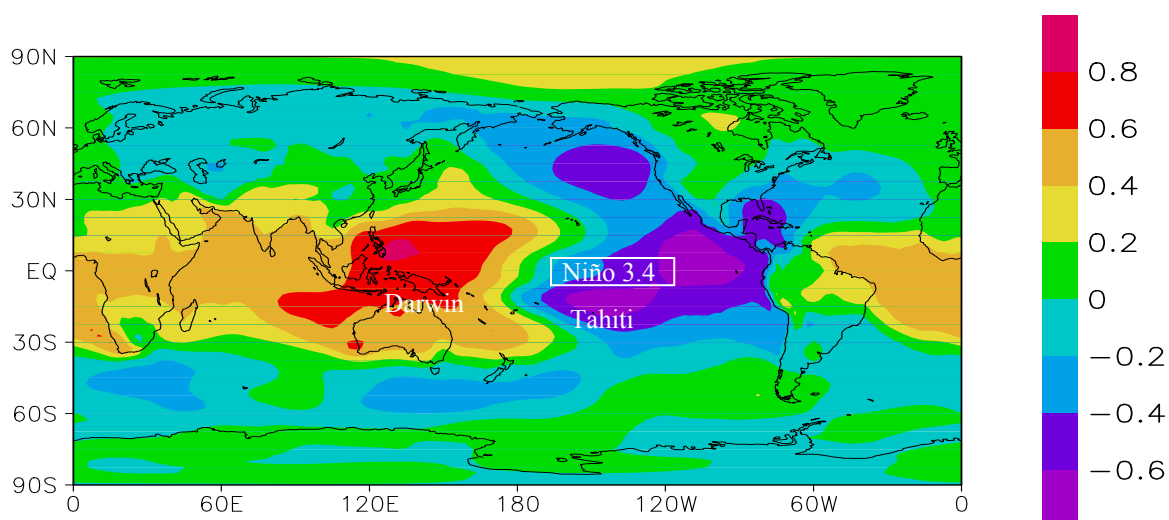


Figure 5.5 Correlation between the sea surface temperature in the eastern tropical Pacific (Niño3.4 index) and sea-level pressure in January. Figure performed on the site <http://climexp.knmi.nl/> (Oldenburg et al., 2004) using NCEP-NCAR **reanalysis**. The approximate locations of the Tahiti and Darwin stations, used to define the SOI, and of the Niño 3.4 box are indicated.

In addition to their effect on the wind stress, the SST **anomalies** related to the ENSO in the Pacific induce an eastward migration of the atmospheric convection (Fig. 5.2) causing higher precipitation in the central Pacific and dry conditions over Indonesia and Northern Australia. ENSO is also associated with perturbations outside the tropical Pacific as it produces anomalies of the atmospheric circulation across nearly the whole

world (Fig. 5.5). For instance, El Niño years tend to be much drier and warmer in Mozambique while the western USA tends to be wetter. Because of these global **teleconnections**, ENSO is probably the internal mode of variability which has the greatest impact on human activities. As a consequence, forecasting its development a few months in advance is an intense area of research.

### 5.2.2 The North Atlantic Oscillation

The large-scale atmospheric circulation in the North Atlantic at mid-latitudes is characterised by westerlies driven by the sea-level pressure difference between the Azores high and the Icelandic low (Fig. 1.5). As described in Section 5.2.1 for the **Walker circulation**, there are irregular changes in the intensity and location of the maxima of these westerlies. This is associated with a North-South oscillation of the pressure, and thus of the atmospheric mass (Fig. 5.6), known as the North Atlantic Oscillation (NAO). The intensity of this mode of variability is measured by the normalised SLP difference between meteorological stations in the Azores and in Iceland:

$$NAO_{index} = \frac{SLP'_{Azores}}{\sigma_{Azores}} - \frac{SLP'_{Iceland}}{\sigma_{Iceland}} \quad (5.2)$$

where  $SLP'_{Azores}$  and  $SLP'_{Iceland}$  are the SLP **anomalies** in the Azores and Iceland and  $\sigma_{Azores}$  and  $\sigma_{Iceland}$  the standard deviations of these **anomalies**. Because of the longer time series available, the station in the Azores is sometimes replaced by one in Portugal. When the NAO index is high, the westerlies are stronger than average while they are weaker than the mean when the NAO index is negative.

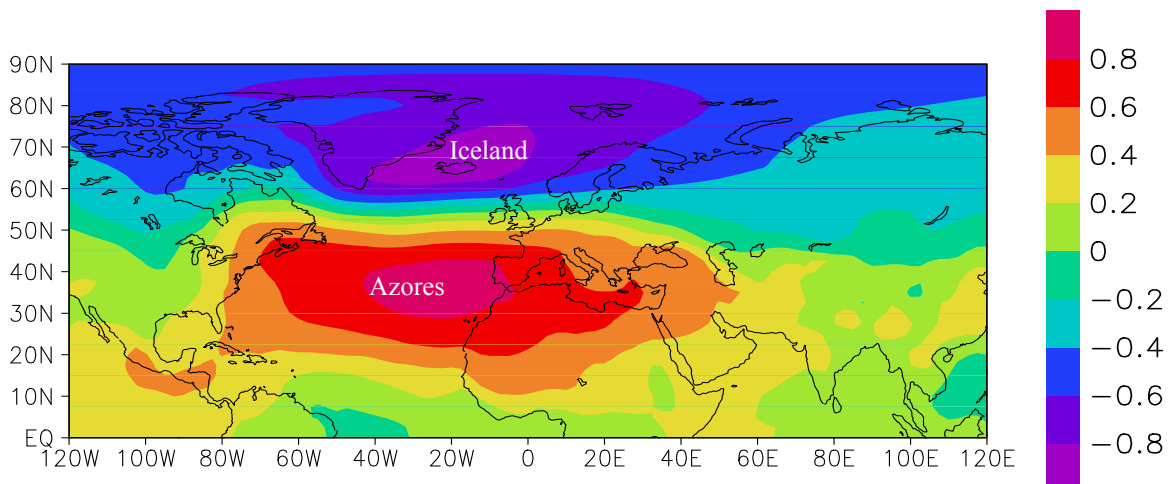


Figure 5.6 Correlation between the winter NAO index and the winter SLP (averaged over December, January, and February). Figure performed on the site <http://climexp.knmi.nl/> (Oldenburg et al., 2004) using NCEP-NCAR **reanalysis**. The location of the Azores and Iceland stations, used to define the NAO index, is indicated.

The NAO can be observed in all seasons, but its amplitude is greater in winter when the atmosphere is more dynamically active. When the NAO index is positive in winter, the strong westerly winds transport warm and moist oceanic air towards Europe. This leads to warming and increased precipitation at mid and high latitudes in Europe as well

as in large parts of northern Asia, the Greenland Sea and the Barents Sea (Fig. 5.7). In the Barents Sea, the warming is associated with a decrease in the sea ice extent.

By contrast, the anomalous circulation when the NAO index is high brings cold air to the Labrador Sea inducing cooling (Fig. 5.7) and an increase in the sea ice extent there. Further southward, the stronger flow around the subtropical high leads to a drop in temperature over Turkey and North Africa and a rise in the eastern US.

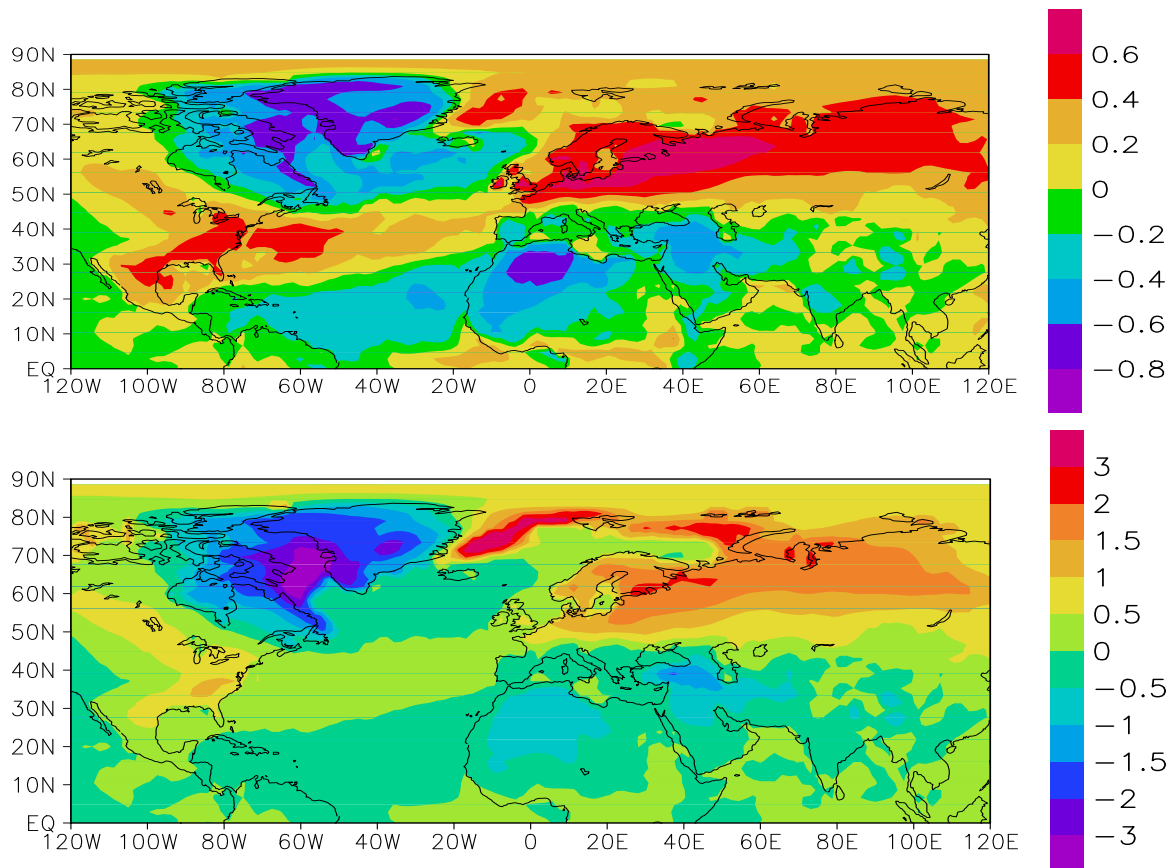


Figure 5.7 Correlation (top) and regression in °C (bottom) between the winter NAO index and the winter surface air temperature (averaged over December, January, and February). Figure performed on the site <http://climexp.knmi.nl/> (Oldenburg et al., 2004) using NCEP-NCAR **reanalysis**.

A tripole is associated with positive NAO index over the Atlantic Ocean: the temperature anomaly is positive around 30°-40°N while it is negative north and south of this latitude band (Fig. 5.7). The dominant cause of this pattern appears to be the air-sea interactions. Indeed, the SSTs tend to be lower in areas where the wind speed is higher, leading to higher evaporation rates and heat losses from the ocean to the atmosphere.

In contrast to the ENSO, which is a coupled ocean-atmosphere mode, the NAO appears to be mainly an intrinsic mode of variability of the atmosphere. It has been found in many types of atmospheric models, whether or not they are coupled to an oceanic layer. The mechanisms governing its existence are related to interactions between the mean and the transient circulation (in particular transient cyclones and anticyclones). However, its amplitude can also be influenced, for instance, by changes in sea surface temperature and by the external forcing (see section 5.5).



Although interesting in its own right, the NAO is sometimes considered as a regional manifestation of a larger scale oscillation of the pressure between subtropical areas and high latitudes. As this nearly-hemispherical mode shows a high degree of **zonal** symmetry, it is referred to as the Northern Annular Mode (NAM, but is also called sometimes the Arctic Oscillation). Like the NAO (with which it is highly correlated), the NAM is associated with changes in the intensity of the westerlies at mid-latitudes.

### 5.2.3 The Southern Annular Mode

The equivalent of the NAM in the Southern Hemisphere is the Southern Annular mode (SAM). Various definitions of SAM have been proposed: a convenient one is the normalised difference in the **zonal** mean sea-level pressure between 40°S and 65°S. As expected, the sea level pressure pattern associated with SAM is a nearly annular pattern with a large low pressure anomaly centred on the South Pole and a ring of high pressure anomalies at mid-latitudes (Fig. 5.8). By **geostrophy**, this leads to an important zonal wind anomaly in a broad band around 55°S with stronger westerlies when SAM index is high.

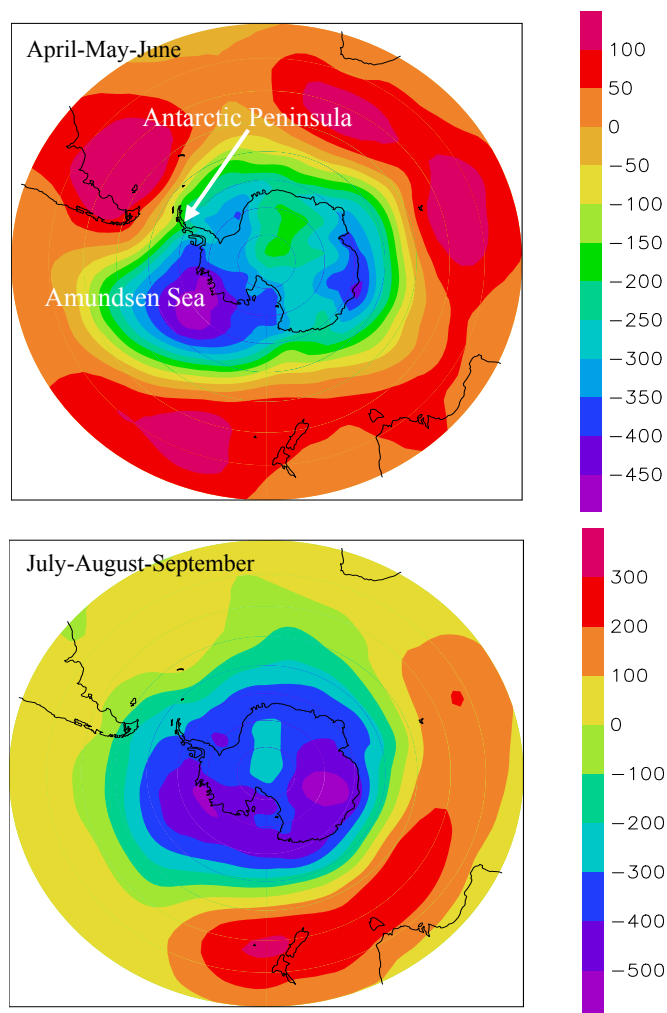


Figure 5.8. Regression between the atmospheric surface pressure and the SAM index for the period 1980-1999 in Pa for (top) the averages in April, May, and June and (bottom) July, August, and September. Data from NCEP-NCAR **reanalyses** (Kalnay et al. 1996).



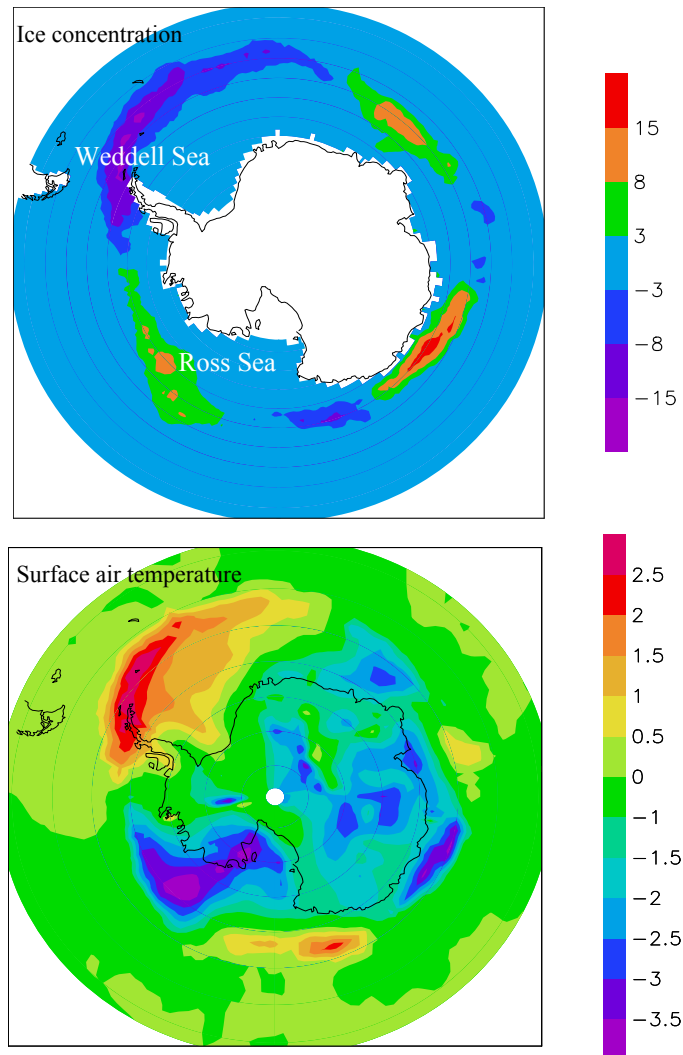


Figure 5.9. Regression between (top) the sea ice concentration in % (data from Rayner et al. 2003) and (bottom) the surface air temperature in °C (Kalnay et al. 1996) and the SAM index averaged over July, August, and September for the period 1980-1999.

Due to the southward shift of the **storm track**, a high SAM index is associated with anomalously dry conditions over southern South America, New Zealand and Tasmania and wet conditions over much of Australia and South Africa. The stronger westerlies above the Southern Ocean also increase the insulation of the Antarctica. As a result, there is less heat exchange between the tropics and the poles, leading to a cooling of the Antarctica and the surrounding seas. However, the Antarctic Peninsula warms due to a western wind anomaly bringing maritime air onto the Peninsula (Fig. 5.9). Indeed, the ocean surrounding the Antarctic Peninsula is in general warmer than the Peninsula itself and stronger westerly winds mean more heat transport onto the Peninsula. Over the ocean, the stronger westerly winds tend to generate stronger eastward currents. Furthermore, the divergence of the currents at the ocean surface around 60°S is enhanced because of a larger wind-induced **Ekman transport**. This results in a stronger oceanic **upwelling** there.

The majority of the effects of SAM could be explained by its annular form and the related changes in **zonal** winds. However, the departures from this annular pattern have large consequences for sea ice as they are associated with meridional exchanges and thus large heat transport. In particular, a low pressure **anomaly** is generally found in the

Amundsen Sea during high SAM-index years (Fig. 5.8). This induces southerly wind **anomalies** in the Ross Sea (Pacific sector of the Southern Ocean) and thus lower temperatures and a larger sea ice extent there (Fig. 5.9). On the other hand, because of the stronger northerly winds, the area around the Antarctic Peninsula is warmer when the ice index is high, and the ice concentration is lower there.

## 5.3 The Climate since the Earth's formation

### 5.3.1 Precambrian climate

To study the Earth's climate during the first billion years of its history, we have to rely on indirect estimates. For instance, the presence of glacial sediments during a particular period indicates glaciation, at least on a regional scale. Specific conditions are required for the formation of various rock types, providing additional indications of past climate changes. However, the uncertainties are very large and the climate reconstructions, which are at best qualitative, are regularly modified as new information becomes available.

Geological Timescale				
Eon	Era	Period	Epoch	Date (million years ago)
Phanerozoic	Cenozoic	Quaternary	Holocene	0,01
			Pleistocene	1,8
		Tertiary	Pliocene	1,8
			Miocene	5,3
			Oligocene	23
			Eocene	34
			Paleocene	56
				65
	Mesozoic	Cretaceous	145	
		Jurassic	199	
		Triassic	251	
		Permian	299	
		Carboniferous	359	
	Paleozoic	Devonian	416	
		Silurian	443	
		Ordovician	488	
		Cambrian	542	
		542		
Precambrian	Proterozoic		2500	
	Archean		4600	

Figure 5.10. A simplified geological time scale. Be careful to the highly non-linear time scale. *Source:* <http://www.naturalsciences.be/active/expeditions/archive2004/china/timescale>. For a more detailed chart, see the site of the International Commission on Stratigraphy: <http://www.stratigraphy.org/>

The evidence for the climate of the early Earth is particularly scarce. When Earth was formed about 4.6 billion years ago, the solar irradiance was about 30% lower than at present. If the conditions (**albedo**, composition of the atmosphere, distance between the Earth and the Sun, etc) then had been the same as they are now, a simple calculation using the models described in Section 2.1.2 leads to an averaged surface temperature 30°C below than today's. During the first 700-800 million years, of Earth's existence, the continual bombardment by small planetesimals and meteorites would certainly have warmed the climate. Nevertheless, in such conditions, the Earth would have been frozen during a large part of its history. This contrasts with geological evidence for a liquid ocean at least 4 billion years ago. The apparent discrepancy is called the "faint early Sun paradox".

The main cause of this paradox is thought to be that there was a much stronger greenhouse effect during the early lifetime of the Earth. The atmosphere was very different from today, with a much higher  $CO_2$  concentration (probably reaching more than 10%, i.e. more than 100 times the present-day value) and nearly no oxygen. In the absence of oxygen, the methane was not quickly oxidised, as in the present atmosphere (see Eq. 2.37), and its concentration was much higher than today. It has been hypothesised that it was the dominant greenhouse gas at this time.

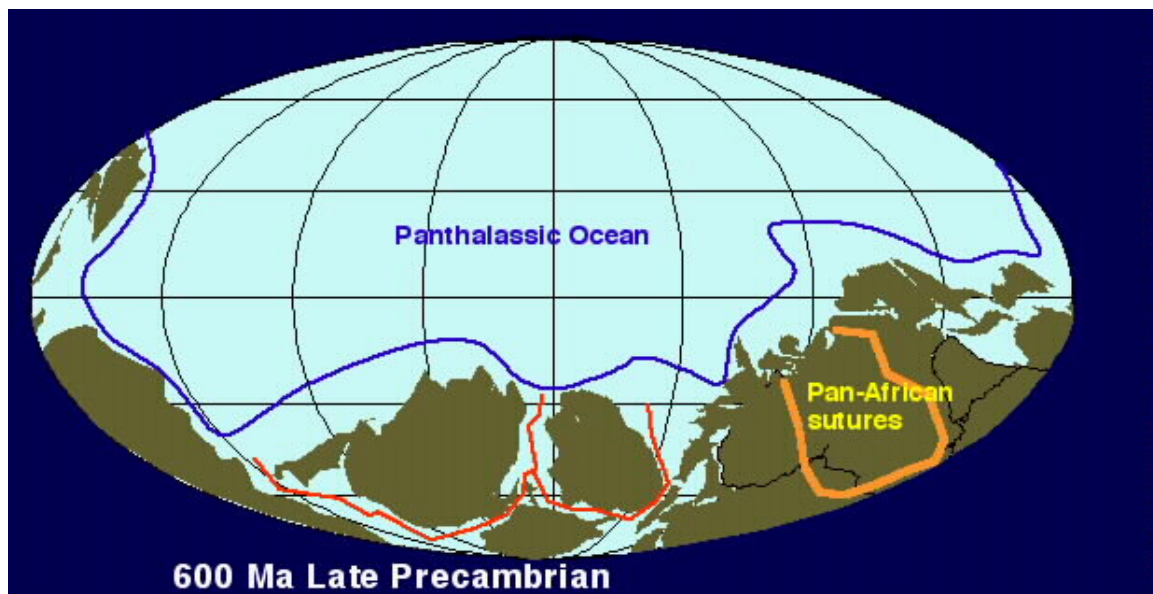


Figure 5.11. Land configuration about 600 million years ago. *Source:* [http://jan.ucc.nau.edu/~rcb7/global\\_history.html](http://jan.ucc.nau.edu/~rcb7/global_history.html). Reproduced with permission.

With time, the atmospheric composition has been modified, in particular because of the oxygen liberated by photosynthesis. This oxygen was first used to oxidise the minerals exposed to the atmosphere. Subsequently, it accumulated in the atmosphere, leading to a large increase in the atmospheric oxygen concentration 2.2. to 2.4 billion years ago as well as to the formation of an **ozone** layer in the stratosphere. Because of these higher oxygen concentrations, the oxidation of methane became more efficient and its concentration decreased markedly. As the rise in the amount of oxygen was concurrent with a glaciation, it has been suggested that the reduced methane concentration was responsible for the cooling. However, the evidence to confirm this hypothesis is still lacking.

Several large climate fluctuations occurred during the Precambrian eon (Fig. 5.10). One of the best documented is a glaciation that takes place around 600 to 750 million

years ago. It was apparently so severe that the whole Earth might have been totally covered by ice during some of this glacial period. At that time, all the continents were grouped close to the South Pole (Fig. 5.11). This maybe have initiated a cooling of the continents, probably during a time when the orbital configuration favoured the growth of ice sheets (see Section 5.4). After this initial cooling, the ice-albedo feedback (see Section 4.2.3) was strong enough to generate an additional temperature decrease leading to a progression of ice towards the Equator and eventually covering the whole Earth.

This “snowball” hypothesis is still debated because it has been argued that such a configuration would be a stable equilibrium state of the climate system, and thus the Earth would have remained permanently frozen. However, it has also been postulated that during the snowball phase, volcanoes would have continued to outgas  $CO_2$  into the atmosphere. As the Earth was covered by ice, no **weathering** of rocks would have compensated the  $CO_2$  input and the atmospheric  $CO_2$  concentration would have increased greatly. Furthermore, ash and dust might have modified the **albedo** of the ice in this very dry environment with very little precipitation. This may have eventually led to a melting of the ice in the tropics and a deglaciation of the Earth thanks to the ice-albedo feedback. Finally, as the  $CO_2$  concentration was still high after this deglaciation, the adjustment of the carbon cycle to such perturbations being very slow, the snowball Earth may have been followed by very warm conditions.

### 5.3.2 Phanerozoic climate

On timescales of millions of years, the carbon cycle is mainly controlled by the exchanges between rocks and surface reservoirs (ocean, atmosphere, biosphere, see Section 2.3.4). As this long-term carbon cycle determines the concentration of atmospheric carbon dioxide ( $[CO_2]$ ), its change over time can be represented in a very simplified way by:

$$\frac{\partial[CO_2]}{\partial t} = Volc(t) - (Weath(t) + Org(t)) \quad (5.3)$$

The first term of the right-hand side of this equation (*Volc*) describes the outgassing of  $CO_2$  associated with **metamorphism** during **subduction** and volcanic eruptions. The second term (*weath*) measures the combined influence of silicate **weathering** and calcium carbonate sedimentation in the ocean, which removes carbon from the atmosphere and the ocean. The last term (*Org*) is associated with long-term burial of organic matter. The imbalance between these three terms has been responsible for changes in the atmospheric  $CO_2$  concentration and the climate for billions of years. Unfortunately, information about the various processes is not precise enough to estimate their magnitude in the Precambrian eon, but the situation is better for the Phanerozoic eon (the last 542 million years).

First, when tectonic activity is intense, high production rates of oceanic crust at the mid-ocean ridges results in more buoyant oceanic plates that push sea water upward. This results in flooding of the low-lying parts of the continents. As such high tectonic activity is related to large **subduction** rates and more frequent/stronger volcanic eruptions, it has been suggested that reconstructions of sea levels can be used to derive the time evolution of the outgassing of  $CO_2$ .

Second, the burial of organic matter can be estimated from the **isotopic** composition of the carbon in sea water. During photosynthesis,  $^{12}C$  is taken preferentially to  $^{13}C$ . This implies that organic matter has a lower content of  $^{13}C$  than the atmosphere or

the ocean. The isotopic composition is commonly measured by delta value  $\delta^{13}C$  which is the ratio of  $^{13}C$  and  $^{12}C$  isotopes in the sample, compared to a reference standard:

$$\delta^{13}C = \left[ \frac{\left( \frac{^{13}C}{^{12}C} \right)_{sample}}{\left( \frac{^{13}C}{^{12}C} \right)_{standard}} - 1 \right] \cdot 1000 \quad (5.4)$$

The past values of  $\delta^{13}C$  in the ocean, which are related to those in the atmosphere at the same period, are recorded in carbonate sediments and can thus be measured. This provides estimates of the rate of burial of organic matter: a larger organic transfer to sediments is associated with a decrease in the relative amount of  $^{12}C$  and thus to an increase in  $\delta^{13}C$ . Based on such measurements, it has been possible to determine that burial was particularly high during the transition the Carboniferous to the Permian period, around 300 million years ago, a period characterised by a relatively large production of fossil fuel-source rocks and relatively low atmospheric  $CO_2$  concentration.

From the information presented above and the estimates of weathering rates based on the exposure of different types of rocks, it is then possible to build models of the long term carbon cycle. Those models can be very complex as they have to estimate the influence of various processes. They can also include, in addition to the carbon cycle, the cycles of other elements such as oxygen or sulphur. However, they still have large uncertainties and some of the hypotheses they use are contentious. For instance, Figure 5.12 illustrates the influence of **climate sensitivity** on the simulated  $CO_2$  concentration in one of these models. **Climate sensitivity** affects the stabilizing feedback between the temperature increase due to higher  $CO_2$  concentration and the intensity of weathering that tends to lower the  $CO_2$  concentration (see section 4.3.2). With low climate sensitivity, this feedback is weak, as  $CO_2$  has only a moderate influence on the climate. As a consequence, the variations of  $CO_2$  concentration are large. By contrast, with high climate sensitivities, the feedback is strong enough to restrain the amplitude of the changes in  $CO_2$ . For the model presented in Figure 5.12, the best agreement with reconstructions of the atmospheric  $CO_2$  concentration based on various **proxy** records is obtained for values of climate sensitivity around  $3^\circ C$ . This is in the middle of the range provided by global climate models for present-day conditions (see Section 4.1.2), suggesting a relative stability of this number over long time scales.

The relatively good agreement between simulated and reconstructed  $CO_2$  concentration gives us some confidence in the proposed interpretation of the dominant factor influencing the long-term carbon cycle. The production rate of oceanic crust by tectonic activity appears to play a particularly important role, since the relatively large divergences that followed the break-up of the super continents around 200 million years ago (super-continent Pangaea) and 550 million years ago (super-continent Pannotia, see Figure 5.11) are associated with significant increases in  $CO_2$  concentration. Furthermore, the periods of low  $CO_2$  concentration generally correspond well with recorded glaciation, for example during the Carboniferous period 300 million years ago. This gives us some confidence in the validity of the simulated and reconstructed  $CO_2$  history, as well as the long term relationship between  $CO_2$  and climate. However, the link between  $CO_2$  and global temperature can not, on its own, explain all the past climate variations, in particular at regional scale. Other factors, such as the location of the continents must also be taken into account, as briefly discussed in Section 5.3.1 above. For instance, when all the continents are grouped together, the interior of the continents tends to be very dry, leading to an extension of desert there.

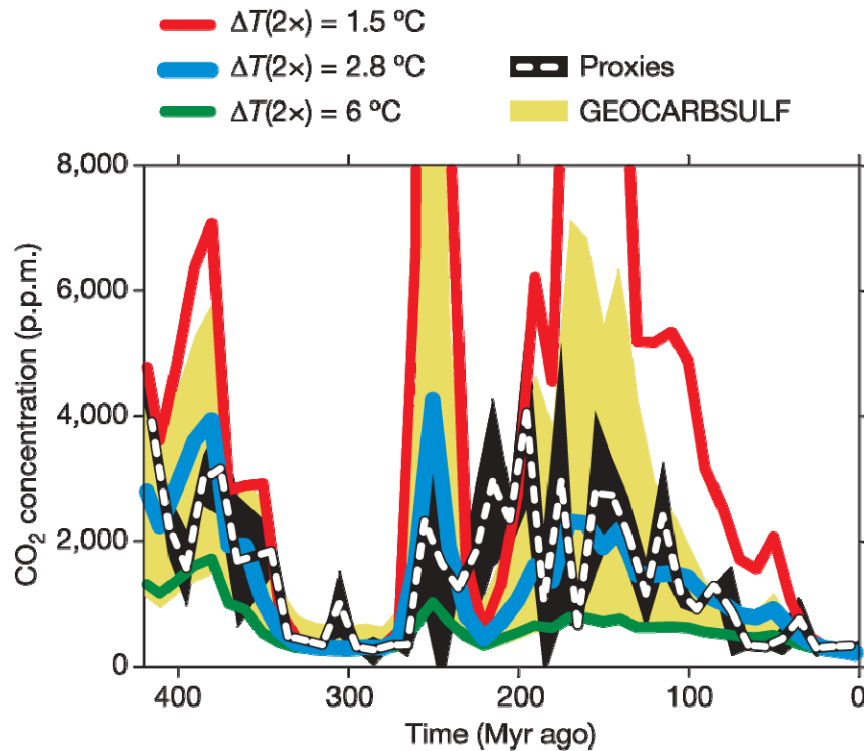


Fig. 5.12. Comparison of the  $CO_2$  concentration calculated by GEOCARBSULF model for varying climate sensitivities (noted  $\Delta T(2x)$  on the figure) to an independent  $CO_2$  record based on different **proxies**. All curves are displayed in 10 million years time-steps. The proxy error envelope (black) represents 1 standard deviation of each time-step. The GEOCARBSULF error envelope (yellow) is based on a combined sensitivity analysis of four different factors used in the model. *Figure from Royer et al. (2007). Reprinted by permission from Macmillan Publishers Ltd: Nature, copyright 2007.*

### 5.3.3 Cenozoic climate

Over the last 65 million years, the  $CO_2$  concentration has gradually decreased from more than 4000 ppmv (part per million in volume) during the Paleocene and the beginning of the Eocene epochs to less than 300 ppmv during the Pleistocene. This long-term decrease is partly due to volcanic emissions, which were particularly large during the Paleocene and Eocene epochs, but which have diminished since then, and to changes in the rate of weathering of silicate rocks. The decline in the  $CO_2$  concentration is associated with a cooling from the warm conditions of the early Eocene climatic optimum between 52 and 50 million years ago (Fig.5.13). This shift is often referred to as a transition from a greenhouse climate to an icehouse, in which ice sheets are present over Antarctica (starting around 35 million years) and over Greenland (starting around 3 million years ago).

Climate reconstructions for this epoch are often based on the oxygen isotopic composition of the shell of small marine organisms called foraminifera (Fig. 5.13). Temperature influences the  $^{18}O/^{16}O$  isotopic fractionation between seawater and the carbonate ions that form the shell. For some species the temperature-fractionation relationship is well known and appears to remain stable with time. So measuring the isotopic composition of the shell remains in sediments provides estimates of past temperatures. This relationship is strictly valid only for ice free conditions since ice

sheets are built from water precipitating at high latitudes which is characterised by a very low  $^{18}\text{O}$  relative abundance. The growth of ice sheets is thus associated with a global decrease in the amount of  $^{18}\text{O}$  available in the other reservoirs, in particular in the ocean. As a consequence, the signal recorded in the shell of foraminifera becomes related to a mixture of temperature and ice-volume influences. In a similar way as for  $^{13}\text{C}$  (Eq. 5.4), the isotopic signal is described using the delta value  $\delta^{18}\text{O}$  defined as:

$$\delta^{18}\text{O} = \left[ \frac{\left( \frac{^{18}\text{O}}{^{16}\text{O}} \right)_{\text{sample}}}{\left( \frac{^{18}\text{O}}{^{16}\text{O}} \right)_{\text{standard}}} - 1 \right] \cdot 1000 \quad (5.5)$$

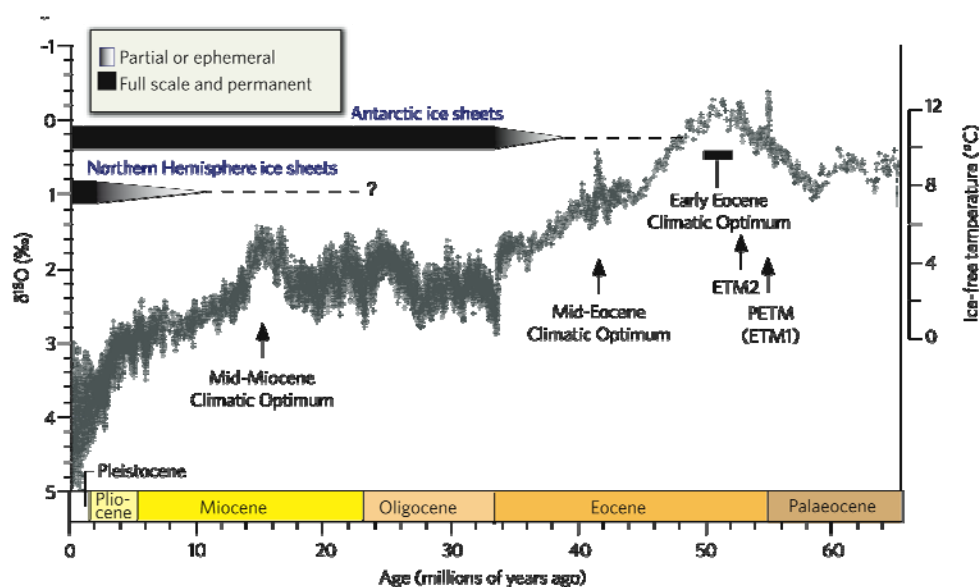


Fig. 5.13 The development of the global climate over the past 65 million years based on deep-sea oxygen-isotope measurements in the shell of benthic foraminifera (i.e. foraminifera living at the bottom of the ocean). The  $\delta^{18}\text{O}$  temperature scale, on the right axis, is only valid for an ice-free ocean. It therefore applies only to the time preceding the onset of large-scale glaciation in Antarctica (about 35 million years ago, see inset in the upper left corner). *Figure from Zachos et al. (2008). Reprinted by permission from Macmillan Publishers Ltd: Nature, copyright 2008.*

60 million years ago, the location of the continents was quite close to that of the present-day one (Fig. 5.14). However, a relatively large seaway was present between North and South America while Antarctica was still connected to South America. The uplift of Panama and the closure of the Central America seaway likely modified the circulation in the Atlantic Ocean, possibly influencing the glaciation over Greenland. More importantly, the opening, deepening and widening of the Drake Passage (between South America and Antarctica) and the Tasmanian Passage (between Australia and Antarctica) allowed the formation of an intense Antarctic Circumpolar Current that isolates Antarctica from the influence of milder mid-latitudes and increased the cooling there. Finally, the uplift of the Himalayas and the Tibetan Plateau strongly modified the monsoon circulation in these regions. Those few examples illustrate the strength of the driving force associated with the changes in boundary conditions due to plate tectonics. This role should not be underestimated.



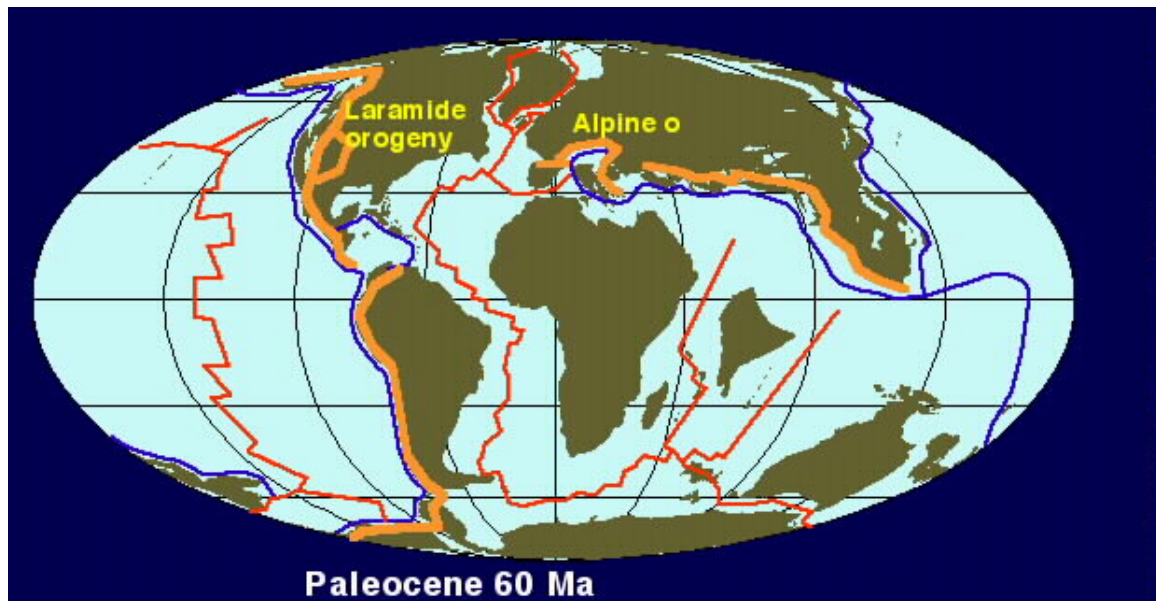


Fig. 5.14. Land configuration about 60 million years ago. *Source* [http://jan.ucc.nau.edu/~rcb7/global\\_history.html](http://jan.ucc.nau.edu/~rcb7/global_history.html). Reproduced with permission.

In addition to the low frequency changes described above, relatively brief events are also recorded in the geological archives. One of the most spectacular is the large meteorite impact that occurred 65 million years ago at the boundary between the Cretaceous and Tertiary periods (or K-T boundary). This cataclysm has been hypothesised to have caused the extinction of many plant and animal species, including the dinosaurs, but its climatic impact is not well known and its long-term influence is not clear. The warming during the Paleocene Eocene Thermal Maximum (PETM, 55 million years ago, see Fig. 5.13), which also had a major impact on life on Earth, is better documented. During this event which lasted less than 170 000 years, the global temperature increased by more than 5°C in less than 10 000 years. This period is also characterised by a massive injection of carbon into the atmosphere-ocean system as recorded by variations in the  $\delta^{13}C$  measured in sediments. The source of these massive inputs of carbon remains uncertain. It may be related to volcanism, or to the release of the methane stored in the sediments of the continental margins. Alternatively, the methane in these regions may have been destabilised by the initial warming, resulting in a strong positive feedback.

Closer to the present, large climate fluctuations have occurred over the last 5 million years. This is not clear on the scale of Figure 5.13, but a higher resolution plot shows fluctuations with a dominant period of 100 000 years over last million years and 41 000 years before that (Fig. 5.15). Those periodicities are very likely related to variations in the insolation, as discussed below.

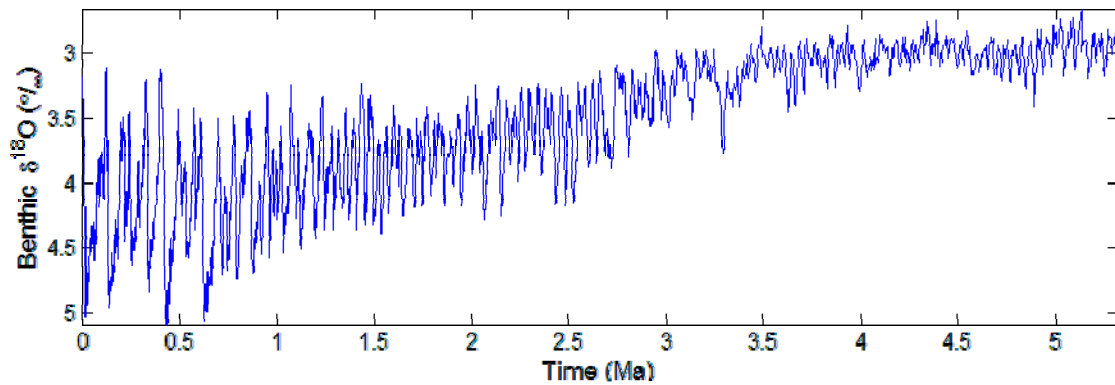


Fig. 5.15. Benthic  $\delta^{18}O$ , which measures global ice volume and deep ocean temperature, over the last 5.3 million years as given by the average of globally distributed records. *Data* from Lisiecki and Raymo (2005). *Source* <http://www.lorraine-lisiecki.com/stack.html>. Reproduced with permission.

## 5.4 The last million years: glacial interglacial cycles

### 5.4.1 Variations in orbital parameters and insolation

If we ignore the role of the atmosphere, the **insolation** at a particular time and location at the Earth's surface is a function of the Sun-Earth distance and the cosine of the solar zenith distance (Eq. 2.20). These two variables can be computed from the time of day, the latitude, and the characteristics of the Earth's orbit. In climatology, the Earth's orbit is determined by three **orbital parameters** (Fig. 5.16 and 5.17): the **obliquity** ( $\epsilon_{obl}$ ) measuring the tilt of the ecliptic compared to the celestial equator (Fig. 2.7), the **eccentricity** ( $ecc$ ) of the Earth's orbit around the sun and the **climatic precession** ( $ecc \sin \tilde{\omega}$ ) which is related to the Earth-Sun distance at the summer solstice. In this definition of the climatic precession,  $\tilde{\omega}$  is the true longitude of the **perihelion** measured from the moving vernal equinox ( $\tilde{\omega} = \pi + PERH$  on Fig. 2.8).

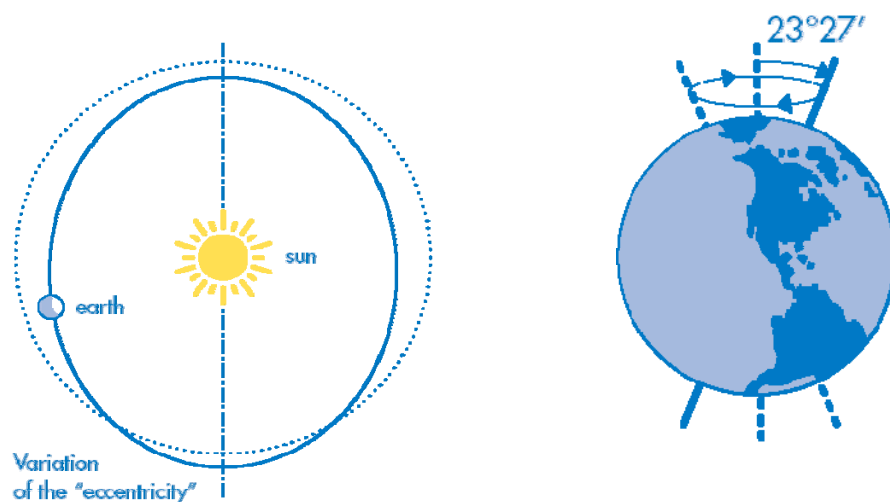


Figure 5.16 Schematic representation of the changes in the eccentricity  $ecc$  and the obliquity  $\epsilon_{obl}$  of the Earth's orbit. *Source*: Latsis foundation (2001)

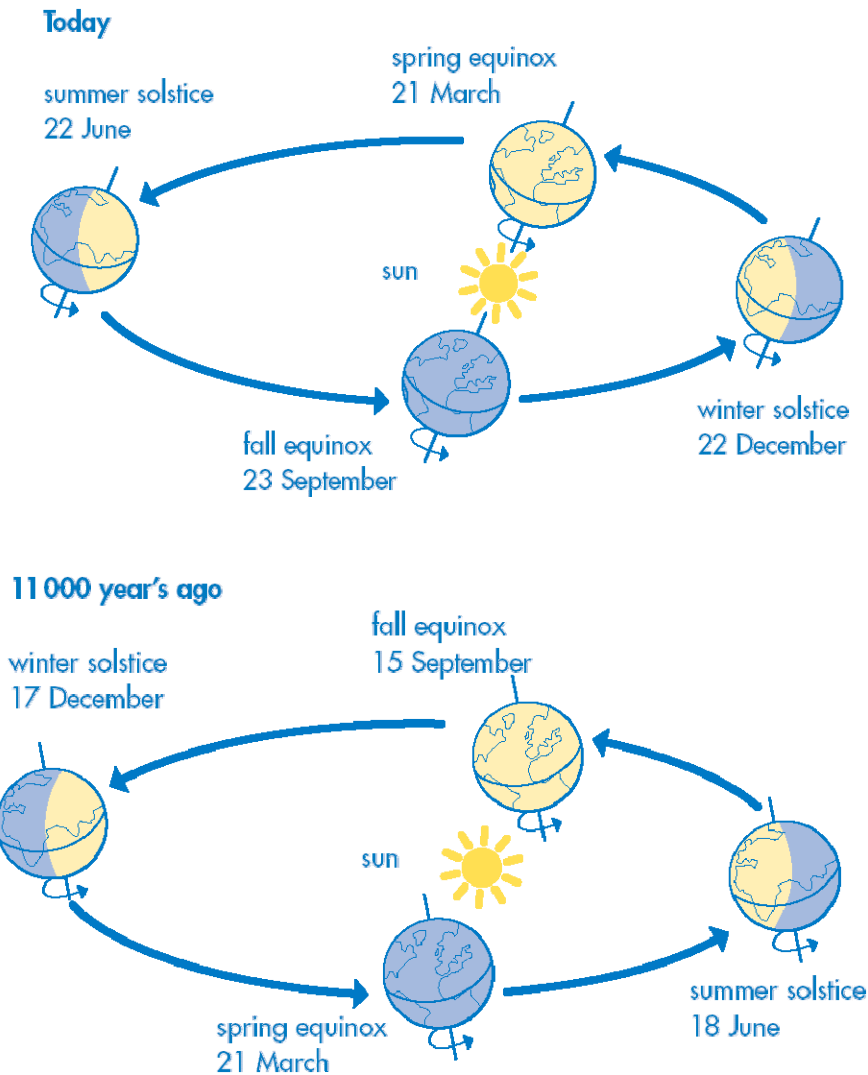


Figure 5.17. Because of the **climatic precession**, the Earth was closest to the Sun during the boreal summer 11 ka ago while it is closest to the Sun during the present boreal winter. *Source*: Latsis foundation (2001)

Because of the influence of the Sun, the other planets in the solar system and the Moon, the orbital parameters vary with time. In particular, the torque applied to the Earth by the Sun and the Moon because our planet is not a perfect sphere (the distance from the surface to the Earth's centre is larger at the Equator than at the poles) is largely responsible for the variations of the obliquity and plays an important role in the changes in  $\tilde{\omega}$ . The eccentricity is particularly influenced by the largest planets of the solar system (Jupiter and Saturn), which also have an impact on  $\tilde{\omega}$ .

The way those parameters have developed over time has been calculated from the equations representing the perturbations of the Earth-Sun system due to the presence of other celestial bodies and to the fact that the Earth is not a perfect sphere. The solution can then be expressed as the sum of various terms:

$$\begin{aligned}
ecc &= ecc_0 + \sum_i E_i \cos(\lambda_i t + \phi_i) \\
\varepsilon_{obl} &= \varepsilon_{obl,0} + \sum_i A_i \cos(\gamma_i t + \xi_i) \\
e \sin \tilde{\omega} &= \sum_i P_i \cos(\alpha_i t + \eta_i)
\end{aligned}
\tag{5.3}$$

The values of the independent parameters  $ecc_0$ ,  $e_{obl,0}$ , of the amplitudes  $E_i$ ,  $A_i$ ,  $P_i$ , of the frequencies  $\lambda_i$ ,  $\gamma_i$ ,  $\alpha_i$ , and of the phases  $\phi_i$ ,  $\xi_i$ ,  $\eta_i$  are provided in Berger (1978), updated in Berger and Loutre (1991). Equations 5.3 clearly show that the orbital parameters vary with characteristic periods (Fig. 5.18). The dominant ones for the eccentricity are 413, 95, 123 and 100 ka. For the climatic precession, the dominant periods are 24, 22, and 19 ka and for the obliquity 41 and 54 ka. To completely determine the Earth's orbit, it is also necessary to specify the length of the major axis of the ellipse. However, taking it as a constant is a very good approximation at least for the last 250 million years

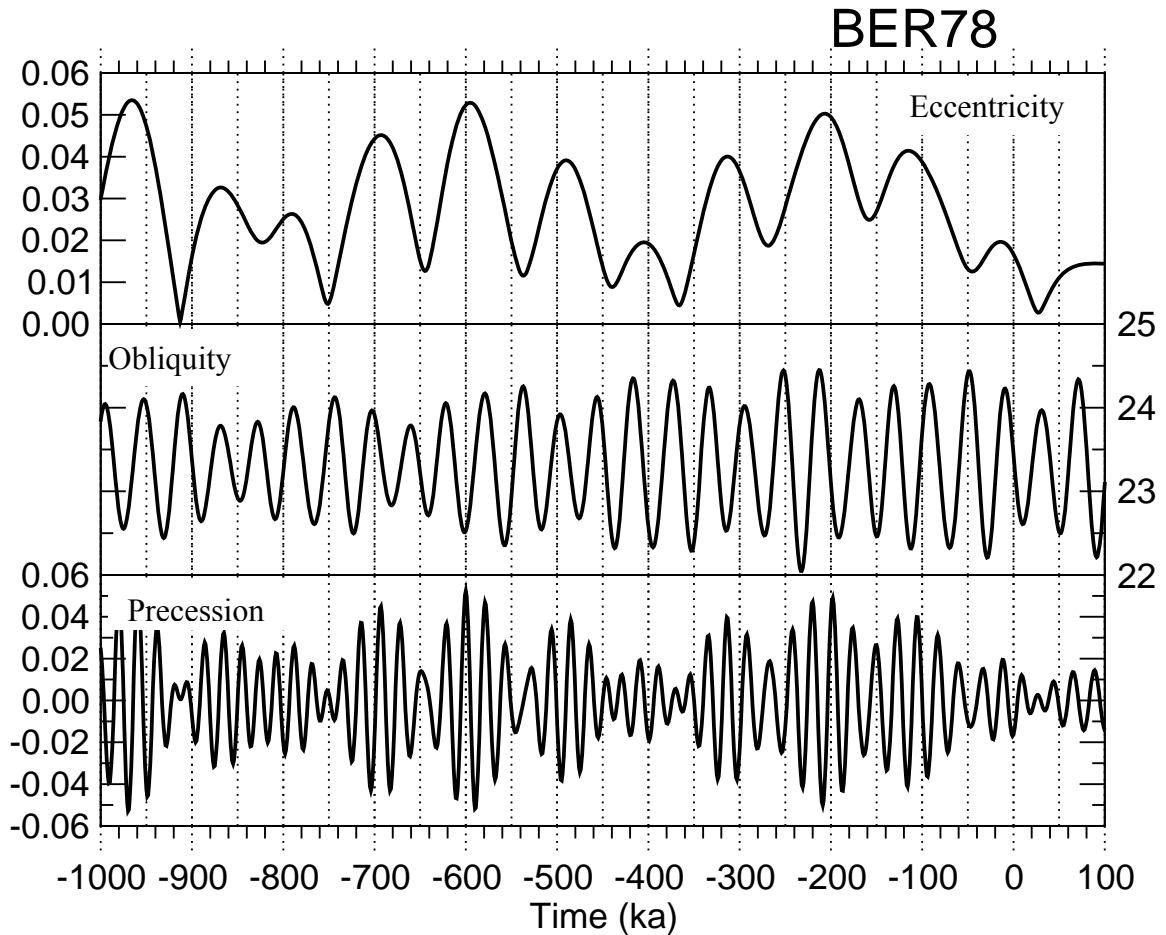


Figure 5.18. Long-term variations in eccentricity, climatic precession and obliquity (in degrees) for the last million years and the next 100 thousand years (zero corresponds to 1950 AD). The minimum value of the climatic precession corresponds to boreal winter (December) solstice at perihelion. computed from Berger (1978).

The eccentricity of the Earth's orbit (Fig.5.16) has varied over the last million years between nearly zero, corresponding nearly to a circular orbit, to 0.054 (Fig. 5.18). Using Eq. 2.24, it can be shown that the annual mean energy received by the Earth is inversely

proportional to  $\sqrt{1-ecc^2}$ . As expected, this value is independent of the obliquity because of the integration over all latitudes, and is independent of  $\tilde{\omega}$  because of the integration over a whole year. The annual mean energy received by the Earth is thus at its smallest when the Earth's orbit is circular and increases with the eccentricity. However, as the variations in eccentricity are relatively small (Fig. 5.18), there are only minor differences in the annual mean radiations received by the Earth. The maximum relative variation is 0.15% ( $1.5 \cdot 10^{-3} = 1 - 1/\sqrt{1-0.054^2}$ ), corresponding to about  $0.5 \text{ W m}^{-2}$  ( $0.5 = 1.5 \cdot 10^{-3} \times 342 \text{ W m}^{-2}$ ).

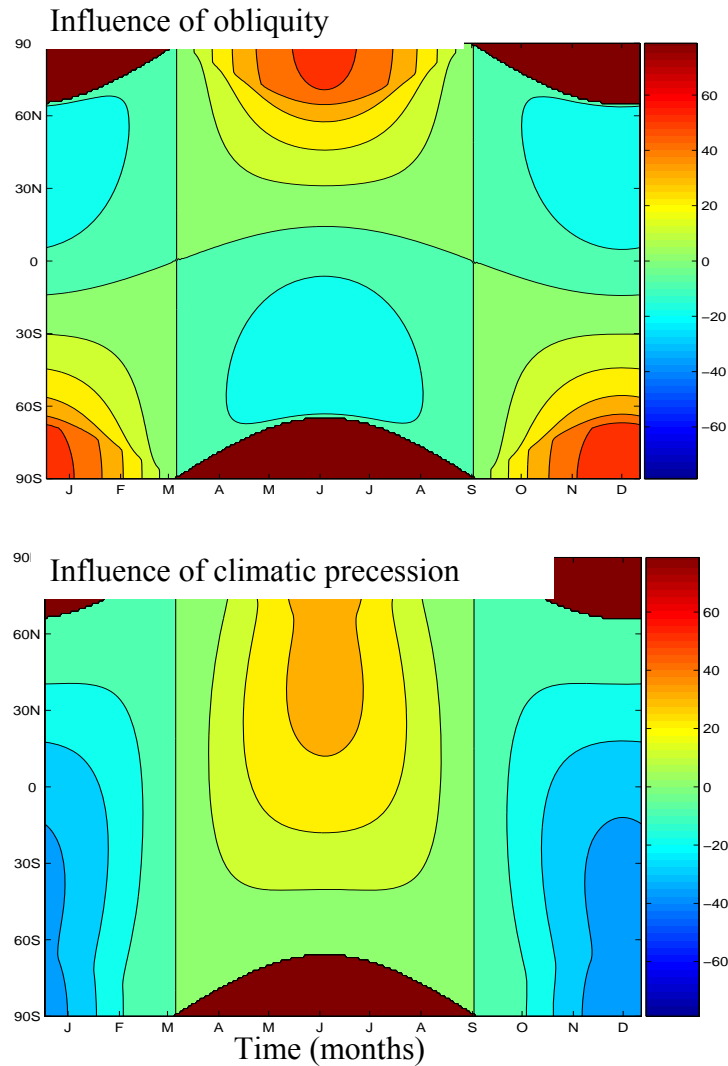


Figure 5.19. Changes in the seasonal contrast of insolation in  $\text{W m}^{-2}$  caused by (top) following an increase in the obliquity from  $22.0^\circ$  to  $24.5^\circ$  with  $ecc=0.016724$ ,  $PERH=102.04$ , i.e. the present-day values, and (bottom) following an increase of the climatic precession from its minimum value (boreal winter at perihelion) to its maximum value (boreal summer at perihelion) with  $ecc=0.016724$ ,  $\varepsilon_{obl}=23,446^\circ$ , i.e. the present-day values. Contour interval is  $10 \text{ W m}^{-2}$ . The brown areas correspond to zone with a zero insolation. Time of the year is measured in term of true longitude  $\lambda_t$ . It is assumed that  $\lambda_t=-80^\circ$  corresponds to the 1<sup>st</sup> of January and one month corresponds to  $30^\circ$  in true longitude.

The obliquity is responsible for the existence of seasons on Earth. If  $\epsilon_{obl}$  were equal to zero night and day would be 12 hours long everywhere (Eq. 2.20 and 2.22) and if  $ecc$  were also equal to zero, each point on Earth would have the same daily mean **insolation** throughout the year (Eq. 2.20 and 2.24). With a large obliquity, the **insolation** is much higher in polar regions in summer, while it is zero in winter during the polar night. Over the last million years, the obliquity has varied from  $22^\circ$  to  $24.5^\circ$  (Fig. 5.18). This corresponds to maximum changes in daily mean **insolation** at the poles of up to  $50 \text{ W m}^{-2}$  (Fig. 5.19). Obliquity also has an influence on the annual mean insolation, increasing it by a few  $\text{W m}^{-2}$  at high latitudes and decreasing it (but to a lesser extent) at the Equator.

Finally, the position of the seasons relative to the perihelion (i.e., the precession) also has an influence on insolation. If Earth is closer to the Sun during the boreal summer and further away during the boreal winter, the summer in the northern hemisphere will be particularly warm and the winter particularly cold. On the other hand, if the Earth is closer to the Sun during boreal winter, the seasonal contrast will be smaller in the northern hemisphere. This effect is particularly marked if the eccentricity is large. If the eccentricity is nearly zero, the distance between the Earth and the Sun is nearly constant, implying no impact of the changes in the position of the seasons relative to the perihelion. The climatic precession varies roughly between  $-0.05$  and  $0.05$ . This produces changes in **insolation** that can be greater than  $20 \text{ W m}^{-2}$  at all the latitudes (Fig. 5.19). As a consequence, the climatic precession dominates the variations of insolation at low and mid latitudes.

#### 5.4.2 The orbital theory of paleoclimates

The information recorded in ice cores (Fig. 5.20) documents the alternation between long glacial periods (or Ice Ages) and relatively brief **interglacials** over the last 800 ka. We are currently living in the latest of these **interglacials**, the **Holocene**. The glacial period that is the best known is the latest one, which peaked around 21 ka BP, and is referred to as the Last Glacial Maximum (LGM). At that time, the ice sheets covered the majority of the continents at high northern latitudes, with ice sheets as far south as  $40^\circ\text{N}$ . Because of the accumulation of water in the form of ice over the continents, the sea level was lower by around 120 m, exposing new land to the surface. For instance, there was a land bridge occurred between America and Asia across the present-day Bering Strait and another between continental Europe and Britain. The **permafrost** and the **tundra** stretched much further south than at present while rain forest was less extensive. Tropical regions were about  $2\text{-}4^\circ\text{C}$  cooler than now over land and probably over the oceans as well (Fig. 5.21). The cooling was greater at high latitudes and the sea-ice extended much further in these regions. Overall, the global mean temperature is estimated to have been between  $4$  and  $7^\circ\text{C}$  lower than at present.

The orbital theory of paleoclimates assumes that the alternations of glacial and interglacial periods are mainly driven by the changes of the orbital parameters with time. In this context, the summer insolation at high northern latitudes, where the majority of the land masses are presently located, appears to be of critical importance. If it is too low, the summer will be cool and only a fraction of the snow that has fallen over land at high latitudes during winter will melt. As a consequence, snow will accumulate from year to year, after thousands of years large ice sheets (See section 4.2), characteristic of the glacial periods, will form. Conversely, if summer insolation is high, all the snow on land will melt during the relatively warm summer and no ice sheet can form. Furthermore, because of the summer warming, snow melting over existing ice sheet can exceed winter accumulation leading to an ice sheet shrinking and a deglaciation. Through this feedback (and other ones, see Chapter 4), the effect of relatively small changes in **insolation** can be amplified, leading to the large variations observed in the glacial-interglacial cycles.

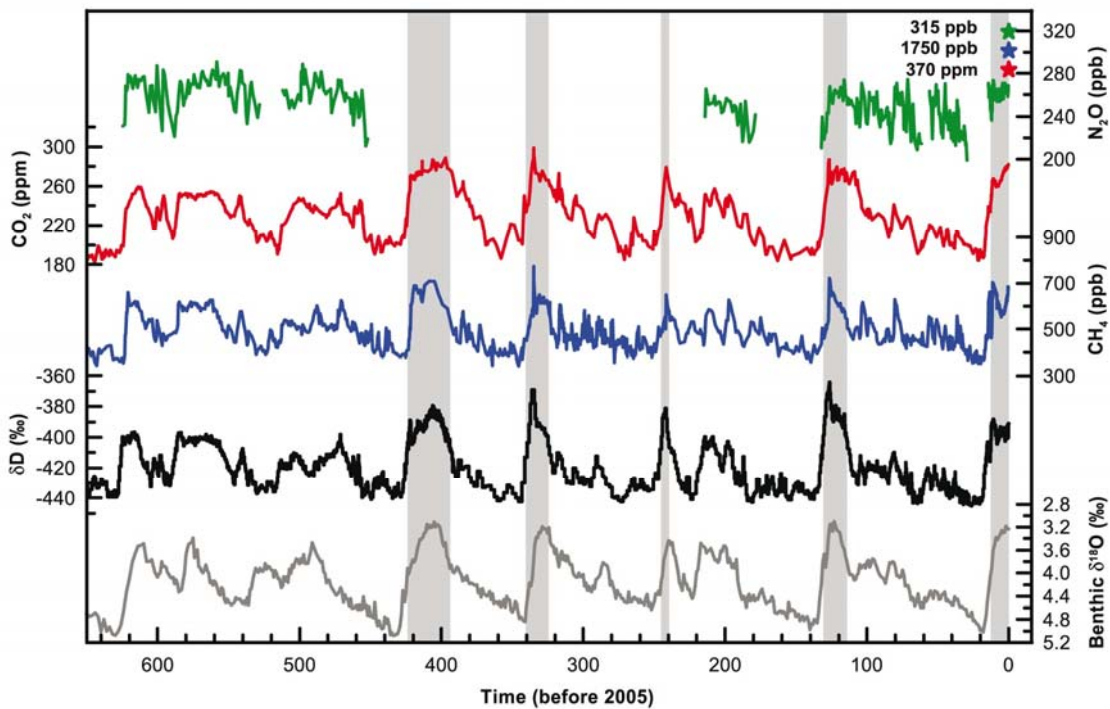


Figure 5.20 Variations in deuterium ( $\delta D$ ; black), and in the atmospheric concentrations of the greenhouse gases  $CO_2$  (red),  $CH_4$  (blue), and nitrous oxide ( $N_2O$ ; green) derived from air trapped within ice cores from Antarctica and from recent atmospheric measurements. The grey curve is a compilation of benthic  $\delta^{18}O$  marine records from various sources. Deuterium is a **proxy** for local temperature, (here for the temperature in Antarctica) and benthic  $\delta^{18}O$  is a proxy for the global ice volume fluctuations, a high value of benthic  $\delta^{18}O$  corresponding to a low ice volume (see Section 5.3.3). The stars and labels indicate the atmospheric concentrations in the year 2000. The shading indicates the last interglacial warm periods. *Source:* Figure 6.3 from Jansen et al. (2007). using a modified legend, published in: *Climate Change 2007: The Physical Science Basis. Contribution of Working Group I to the Fourth Assessment Report of the Intergovernmental Panel on Climate Change*, Cambridge University Press, copyright IPCC 2007. Reproduced with permission.

One of the most convincing arguments for the orbital theory of paleoclimate comes from the fact that the dominant frequencies of the orbital parameters are also found in many proxy records of past climate change (e.g. Fig. 5.20). This suggests a strong causal link. Another important argument comes from paleoclimate modelling. A climate model driven by changes in orbital parameters and by the observed evolution of greenhouse gases over the last 600 ka reproduced quite well the estimated past ice volume variations. If the changes in orbital parameters were not taken into account, it was not possible to simulate adequately the pace of glacial-interglacial cycles (Fig. 5.22).



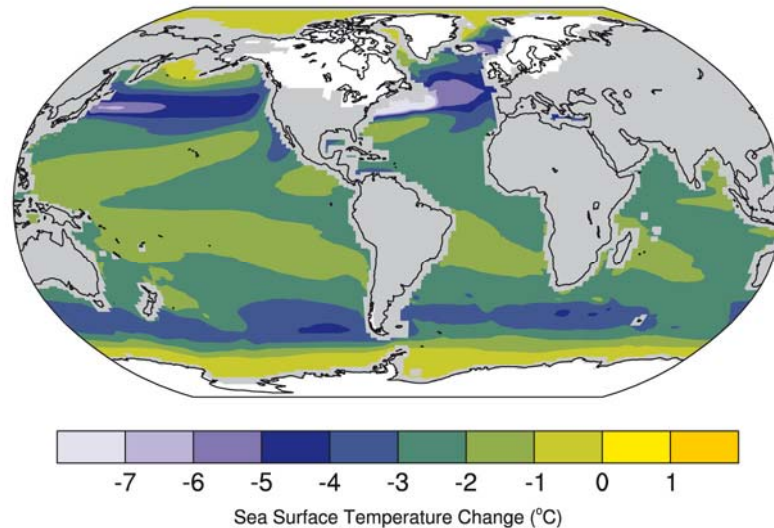


Figure 5.21 Multi-model average change in SST between the Last Glacial Maximum climate (approximately 21 ka ago) and the pre-industrial (1750 AD) climate. Ice extent over continents is shown in white. The selected model results were compiled in the framework of the PMIP2 project (<http://pmip2.lsce.ipsl.fr/>). Figure 6.5 from Jansen et al. (2007). using a modified legend, published in: Climate Change 2007: The Physical Science Basis. Contribution of Working Group I to the Fourth Assessment Report of the Intergovernmental Panel on Climate Change, Cambridge University Press, copyright IPCC 2007. Reproduced with permission.

However, the link between climate change and **insolation** is far from being simple and linear. In particular, the correspondence between summer insolation at high latitudes and ice volume is not clear at first sight (e.g. Fig. 5.22). It appears that ice sheets can grow when summer **insolation** is below a particular threshold (see, for instance, the low value around 120 ka BP when the last glaciation started). On the other hand, because of the powerful feedbacks, in particular related to the presence of ice sheets (see Chapter 4), the insolation has to be much stronger to induce a deglaciation. The insolation also changes in different ways at every location and every season, making the picture more complex than that presented by a simple analysis of the summer **insolation** at high latitudes.

One of the most intriguing points is the predominance of strong glacial-interglacial cycles with a period of around 100 ka while this period is nearly absent from the insolation curves. The eccentricity does exhibit some dominant periods around 100 ka but it is associated with very small changes in **insolation**. Furthermore, until 1 million years ago, the ice volume mainly varied with a period of 40 ka, corresponding to the dominant period of the **obliquity** (Fig. 5.15). The importance of the 100 ka cycle over the last million years is probably related to some non-linear processes in the system. However, explaining the mechanisms involved in detail and in a convincing way is still a challenge.

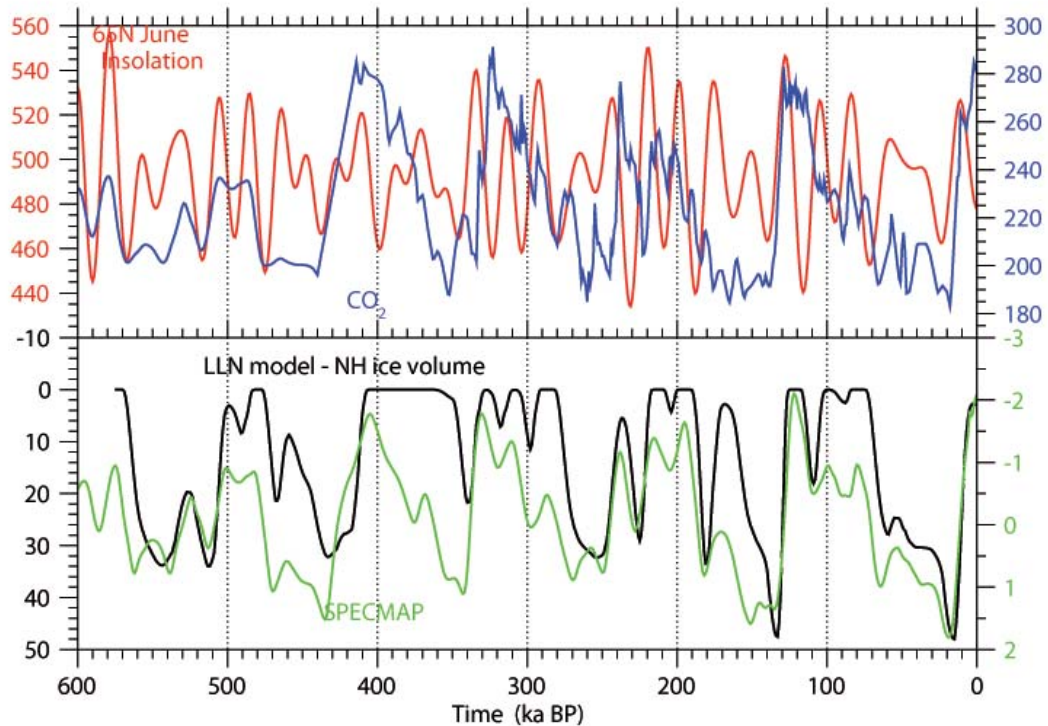


Figure 5.22 (Top panel) The atmospheric CO<sub>2</sub> concentration (in ppm, blue) (as measured in the Vostok ice core over the last 414 ka (Petit et al., 1999) plus a statistical scenario for earlier dates) and the mid-month insolation value at 65°N at the June solstice (in Wm<sup>-2</sup>, red) according to (Berger, 1978). (Bottom panel) The Northern Hemisphere ice volume (in 10<sup>6</sup> km<sup>3</sup>) simulated by the LLN 2-D climate model (Berger and Loutre, 2003) forced by insolation (Berger, 1978) and atmospheric CO<sub>2</sub> concentration (as in top panel) and SPECMAP curve (stacked, smoothed oxygen-isotope record in deep sea cores, Imbrie et al., 1984)

### 5.4.3 Glacial-interglacial variations in the atmospheric CO<sub>2</sub> concentration

The greenhouse gas concentrations have varied nearly synchronously with temperature and ice volume over the last 600 ka at least (Fig. 5.20) with the difference between interglacial and glacial periods reaching about 80 ppm for carbon dioxide and 300 ppb for methane. This corresponds to a radiative forcing of nearly 3 W m<sup>-2</sup> and thus to a strong amplifying mechanism for the cooling during glacial periods. However, as mentioned in the latest IPCC report, “the qualitative and mechanistic explanation of these CO<sub>2</sub> variations remains one of the major unsolved question in climate research” (Jansen et al. 2007).

The land biosphere cannot be responsible for this decrease in the CO<sub>2</sub> concentration during glacial periods. Because of the advance of ice sheets, the land area available for vegetation growth declines significantly. Furthermore, the lower temperatures induce less evaporation over the oceans and less precipitation over land. The fraction of dry areas and desert, which only store a small amount of carbon compared to, for instance, forest is thus larger. All these factors lead to a decrease in the carbon storage over land which was not compensated for by the growth of terrestrial vegetation on the new land area associated with the lower sea level. As a consequence, changes in the land biosphere during glacial

periods tend to increase the atmospheric CO<sub>2</sub> concentration by an amount which is estimated to be around 20 ppm.

The cause of the decline must thus lie in the ocean, the geological processes being too slow to account for the observed changes. Because of the accumulation of freshwater with nearly zero **dissolved organic carbon** and **alkalinity** in the ice sheets, the salinity, *DIC* and *Alk* of the ocean increases. This leads to an increase of pCO<sub>2</sub> in the ocean. However, it can be shown that this is outweighed by the greater solubility of CO<sub>2</sub> in the ocean due to cooling. The net effect is a small decrease in the atmospheric concentration of CO<sub>2</sub>, but it is insufficient to explain all the 80 ppm decrease between interglacial and glacial periods.

This decrease must therefore be related to changes in the ocean circulation and/or the **soft tissue** and **carbonate pumps**. All these factors have a large influence on the distribution of *DIC* and *Alk* in the ocean and thus on the ocean-atmosphere CO<sub>2</sub> exchanges. Most hypotheses emphasises the role of the Southern Ocean. A strong argument in favour of this is the very similar evolution of atmospheric CO<sub>2</sub> concentration and Antarctic temperatures (Fig. 5.20). At present, there is a strong **upwelling** of deep water, rich in nutrients and DIC, in that area. Biological activity is insufficient to fix the excess carbon and some of the carbon coming from the deep ocean is transferred to the atmosphere. If in glacial periods, this upwelling (and more generally the connection between surface and deep water) or the biological production changed, this would have a considerable influence on the concentration of atmospheric CO<sub>2</sub>.

The upwelling might have been reduced at the LGM by of a northward shift of the westerlies in the Southern Ocean, and thus by the divergence associated with the wind-induced **Ekman transport**, but this still needs to be confirmed. The weaker hydrological cycle during cold periods, and the associated increase in the Earth's surface covered by dry areas had probably lead to a greater dust transport towards the Southern Ocean. This had brought a large amount of iron to the Southern Ocean. As a consequence, biological production might have been higher during glacial times as this micro-nutrient strongly limits the primary production for the present-day condition in the area. Both of these effects could thus have played a role in the observed atmospheric CO<sub>2</sub> concentration decrease.

It has also been suggested that the supply of iron to the Southern Ocean by dust have induced a large-scale shift in the ecosystem from phytoplankton producing calcium carbonate towards species which do not form CaCO<sub>3</sub>. This would have decreased the intensity of the **carbonate pump**, so inducing a decrease in the CO<sub>2</sub> concentration.

Many other explanations have been suggested, but it seems that, on its own, none of them can explain the 80 ppm change. It is very likely that some of them play an important role, while others have a negligible influence. However the relative importance of the various explanatory factors is presently unknown.

## 5.5 The Holocene and the last 1000 years

### 5.5.1 The current interglacial

In addition to the low frequency variability of glacial-interglacial cycles, more rapid changes have been observed during the past million years. Those that are best documented, in particular in Greenland ice cores (Fig.5.23), are associated with the millennium-scale variability that took place during the last glacial period. These variations are generally attributed to changes in the oceanic circulation and the oceanic heat transport, implying a large-scale shift in the climate. The deglaciation was also characterised by a strong millennium-scale cooling called the Younger Dryas that

followed a period of warming that peaked around 14 000 years ago. By contrast, the climate of the latest interglacial appears to be relatively stable. Although some fluctuations are observed, their amplitude over Greenland is much smaller than those seen in glacial periods.

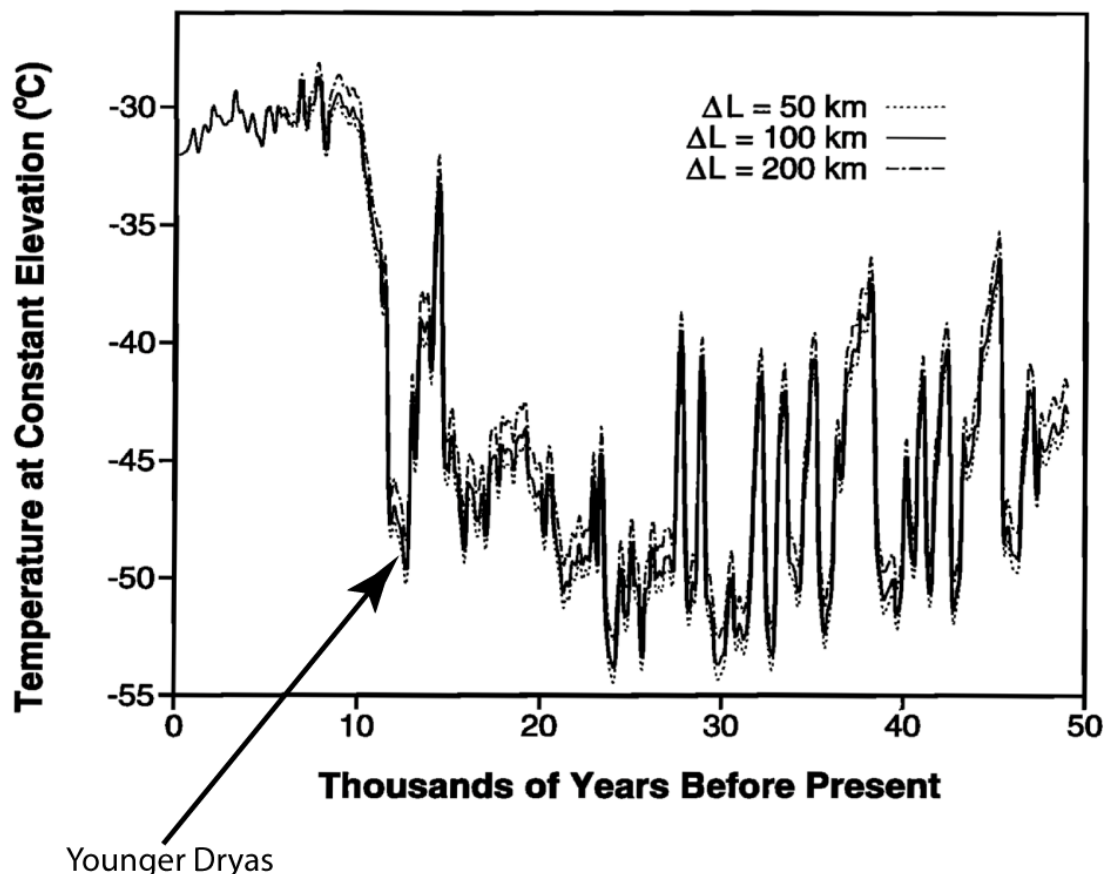


Figure 5.23 Temperature history derived from  $\delta^{18}O$  measurements in Greenland (Greenland Ice Sheet Project 2 ice core), using three different corrections for elevation changes. Be careful that time is going from right to left. Figure from Cuffey and Clow (1997).

Mainly because of the influence of **precession**, the **insolation** at the top of the atmosphere was very different 10 000 years ago than it is at present (Fig. 5.24). In particular, the summer insolation at the North Pole was up to  $50 \text{ W m}^{-2}$  higher than now. As a consequence, the summer temperature in the northern hemisphere was relatively high during the Early Holocene and this period is often referred to as the Holocene Thermal Optimum or Holocene Climatic Optimum. However, the timing of the temperature maximum depends strongly on location, as during the Early Holocene ice sheets were still present over parts of Canada, inducing strong local cooling, and changes in oceanic and atmospheric circulation have a strong influence at the regional scale. Nevertheless, if we ignore the last 150 years for which different forcing were in action (see section 5.5.3), the highest summer temperatures of the Holocene are generally found between 9 and 6 kyr BP.

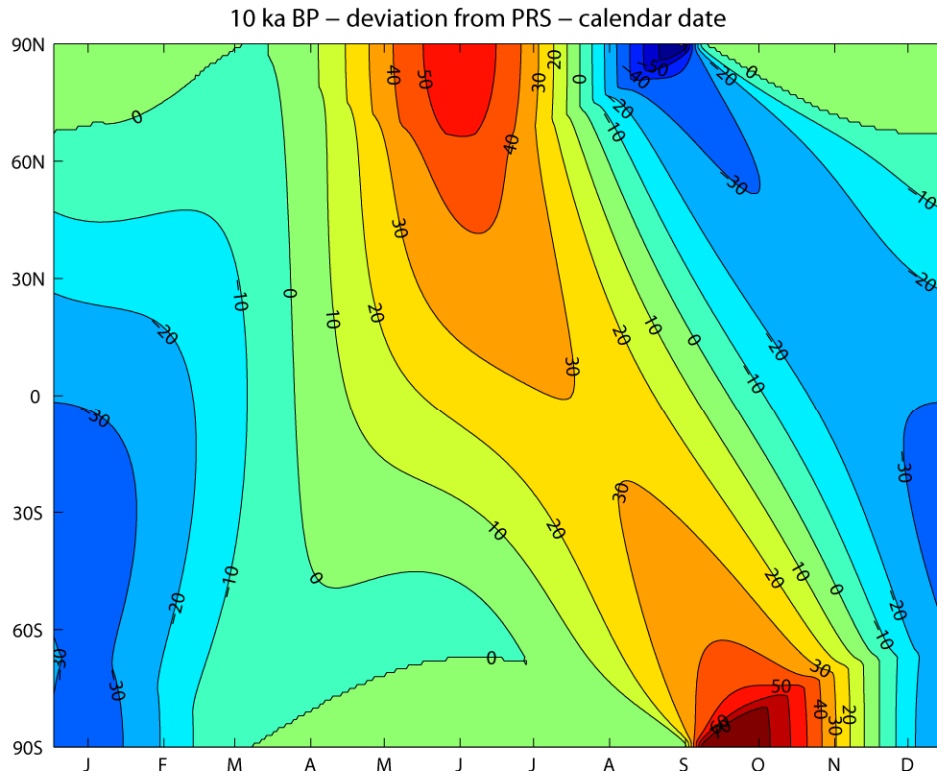


Figure 5.24 Deviations from present-day values of the calendar 24h mean solar irradiance (daily **insolation**) around 10 000 years ago (i.e. at 10ka BP) (in Wm<sup>-2</sup>)

The decrease in Northern Hemisphere **insolation** during the Holocene is associated with a long term summer cooling, which is stronger over land than over the ocean because of the larger seasonal cycle of the temperature over land. As the **monsoons** are strongly influenced by temperature contrasts between land and ocean, this leads to a weakening of the summer **monsoons**. Over North Africa, the weaker monsoon circulation is associated with a marked reduction in precipitation that produced a shift from a Sahara largely covered by savannah and lakes during the Early Holocene to the dry desert state that we know now. The changes in insolation were relatively smooth. However, some studies, mainly those focusing on the Western Sahara, have suggested that the desertification was relatively abrupt, taking place in less than 1000 years about 4000 years ago. This could be due to some **biogeophysical feedbacks** (see Chapter 4) amplifying the initial perturbation caused by radiative forcing. Another hypothesis is that a steep decrease in the vegetation cover can occur if the precipitation crosses a threshold related to the biological characteristics of the plant, leading to a highly non-linear response to changes in precipitation. By contrast, recent observation shows a gradual transition from a “green” to a desert state in the eastern Sahara. Additional work is still needed to understand this important transition in detail.

## 5.5.2 The last 1000 years

### 5.5.2.1 Hemispheric-scale changes

The last millennium is certainly the period in the past for which we have the greatest number of proxy records. Tree rings, lake and marine sediments, ice cores, etc, all provide very useful information on past climate changes. Nevertheless, the uncertainty



over temperature changes is still significant (Fig. 5.25). All the available reconstructions show relatively mild conditions around 1000 AD (the so-called Medieval Warm Period), followed by a cooling that culminated around the 17-19<sup>th</sup> centuries (the so-called Little Ice Age). However, the amplitude and the exact time of the changes vary strongly between the different reconstructions. However, all the reconstructions have their absolute maximum during the 20<sup>th</sup> century.

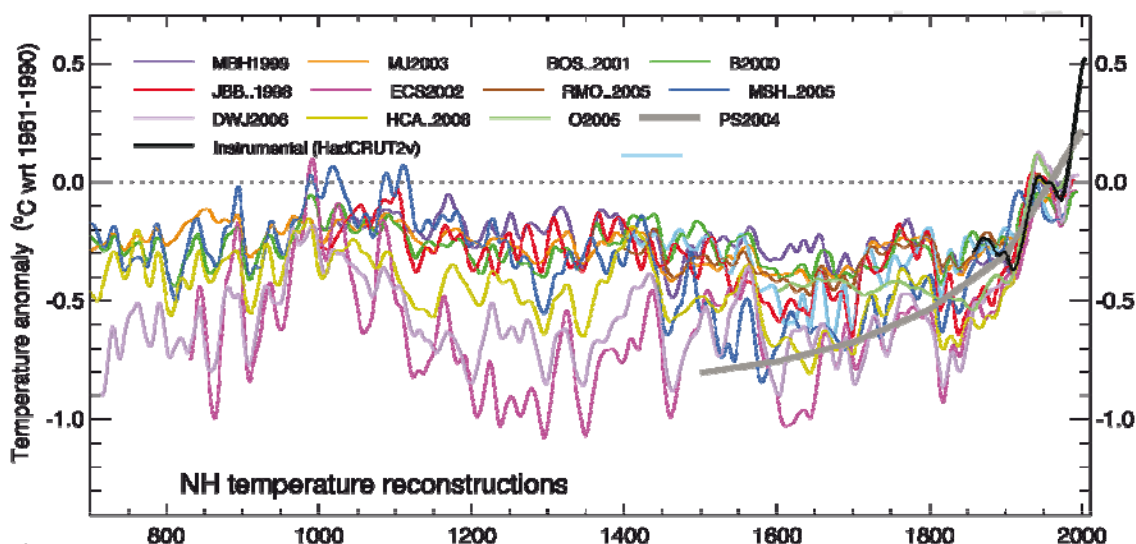


Figure 5.25 Reconstructions of Northern Hemisphere temperature variations over the last 1300 years using multiple climate proxy records and the instrumental record for the last 150 years. All series have been smoothed to remove fluctuations on time scales less than 30 years. All temperatures represent anomalies (°C) from the 1961 to 1990 mean. Figure 6.10 from Jansen et al. (2007), using a modified legend, published in: *Climate Change 2007: The Physical Science Basis. Contribution of Working Group I to the Fourth Assessment Report of the Intergovernmental Panel on Climate Change*, Cambridge University Press, copyright IPCC 2007. Reproduced with permission. See Jansen et al. (2007) for a full reference to all the reconstructions.

When analysing climate changes over periods of the order of several millennia, orbital forcing is generally dominant. However, for shorter periods, such as the last 1000 years, variations in insolation at the top of the atmosphere due to changes in orbital parameters are relatively weak and other forcings have to be taken into account. On these time scales, the two dominant natural forcings are changes in **total solar irradiance** (TSI) and large volcanic eruptions. The majority of volcanic eruptions have a dramatic local impact but only a weak large-scale influence on climate. By contrast, some major eruptions can transport large amounts of aerosols into the stratosphere where they can stay for a few years. These aerosols modify the radiative properties of the atmosphere, decreasing the solar irradiance at the surface and thus lowering the temperature, in particular in summer. In addition, volcanic aerosols have an impact on the atmospheric circulation and tend to favour a positive phase of the North Atlantic Oscillation. As a consequence, a major volcanic eruption is often followed by a warm winter over Europe, a characteristic of a positive NAO index.

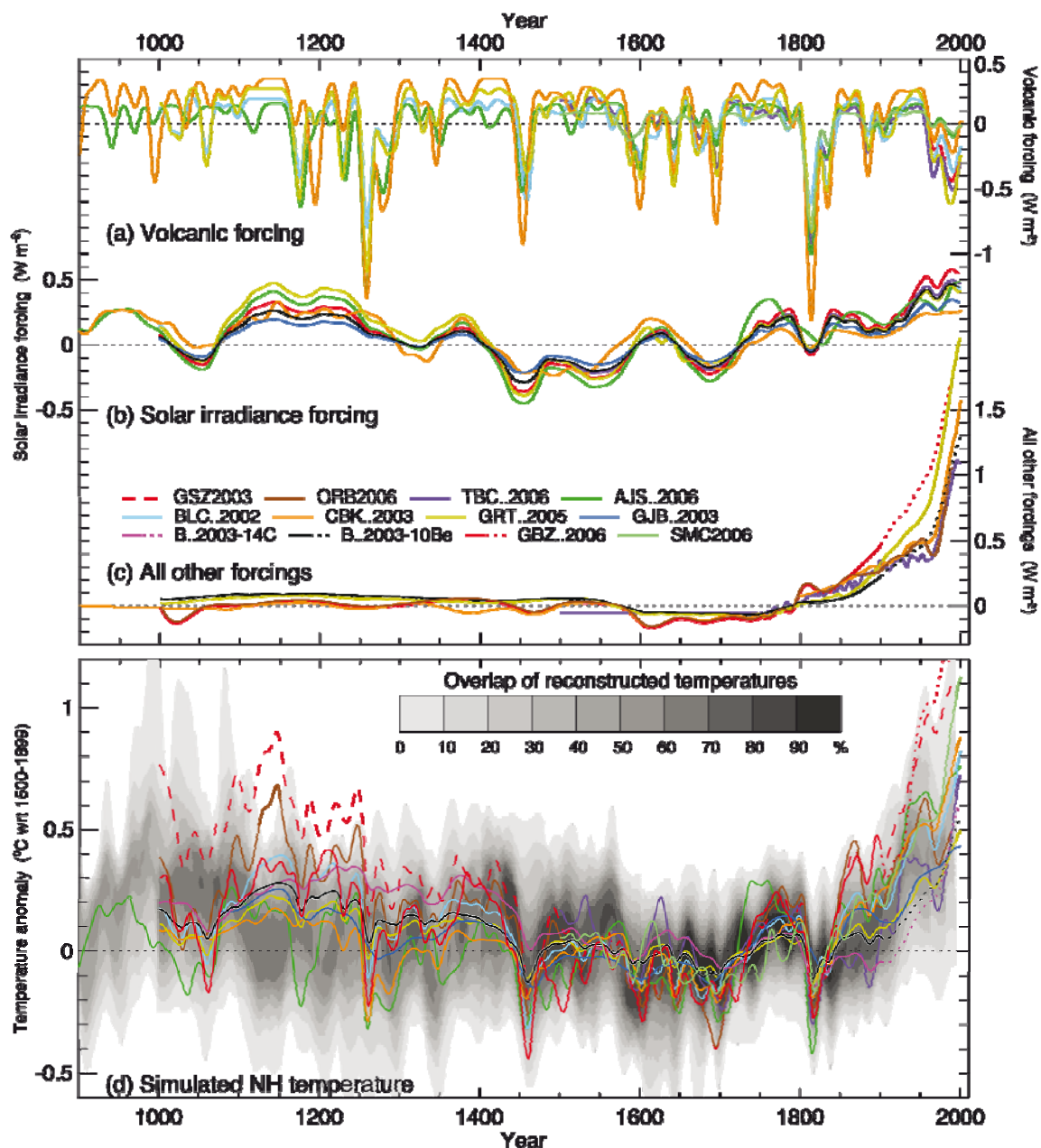


Figure 5.26 Radiative forcings and simulated temperatures during the last 1100 years. The global mean radiative forcing ( $W m^{-2}$ ) used to drive climate model simulations due to (a) volcanic activity, (b) solar irradiance variations and (c) all other forcings (which vary between models, but always include greenhouse gases, and, except for those with dotted lines after 1900, tropospheric sulphate aerosols). (d) Annual mean Northern Hemisphere temperature ( $^{\circ}C$ ) simulated under the range of forcings shown in (a) to (c), compared to the concentration of overlapping Northern Hemisphere temperature reconstructions. All forcings and temperatures are expressed as **anomalies** from their 1500 to 1899 means and then smoothed with a Gaussian-weighted filter to remove fluctuations on time scales less than 30 years. Figure 6.13 from Jansen et al. (2007) using a modified legend, copyright IPCC 2007, reproduced with permission. See Jansen et al. (2007) for a full reference to all the time series.

In contrast to the orbital forcing whose time development is very well known, we are still uncertain about both solar (TSI) and volcanic forcings. On the one hand, the



volume and characteristics of the aerosols released by the volcanic eruptions have to be derived indirectly from the measurements of sulphate loads in ice cores (Fig. 5.26). On the other hand, we have precise measurement of TSI from satellites over the last 30 years. For earlier times, measurement of the concentration of cosmogenic isotopes, such as  $^{10}\text{Be}$  and  $^{14}\text{C}$ , in ice cores can be used as a **proxy** for TSI. When solar activity is low, the shielding of the Earth from energetic cosmic ray is weaker, and there is an increase in the production of those isotopes. However, the link between the concentration of cosmogenic isotopes in ice cores, solar activity and solar forcing is far from simple. It has even been suggested that some of the widely used reconstruction (e.g. Fig. 5.26) overestimate the long term changes in TSI by up to a factor five.

The last millennium is an ideal test case for climate models to compare natural and human induced changes. Whether driven by solar and volcanic forcings as well as by anthropogenic forcings (increase in greenhouse gas concentration, sulphate aerosol load, land use changes, see Section 5.5.3), the simulated temperatures are within the range provided by the reconstructions. This gives us some confidence in the validity of models. Furthermore, simulations can be used to analyse the causes of the observed changes. In particular, the cold periods during the Little Ice Age correspond well to times with a relatively low TSI and frequent volcanic eruptions.

### 5.5.2.2 Regional-scale changes

Although the forcings in the last millennium have relatively small amplitudes, they have played a dominant role in the changes in the temperature on a hemispheric scale (Fig. 5.26). By contrast, on a regional scale, changes in the oceanic or atmospheric circulation can completely mask the influence of the forcing in some periods. As a consequence, the Medieval Warm Period and the Little Ice Age can by no means be considered as globally or even nearly globally synchronous phenomena. This is the reason some climatologists avoid using these terms. The temperature in the first part of the second millennium was generally higher than in the period 1500-1900 but warm and cold periods occurred at different times in different locations (e.g., Fig. 5.27).

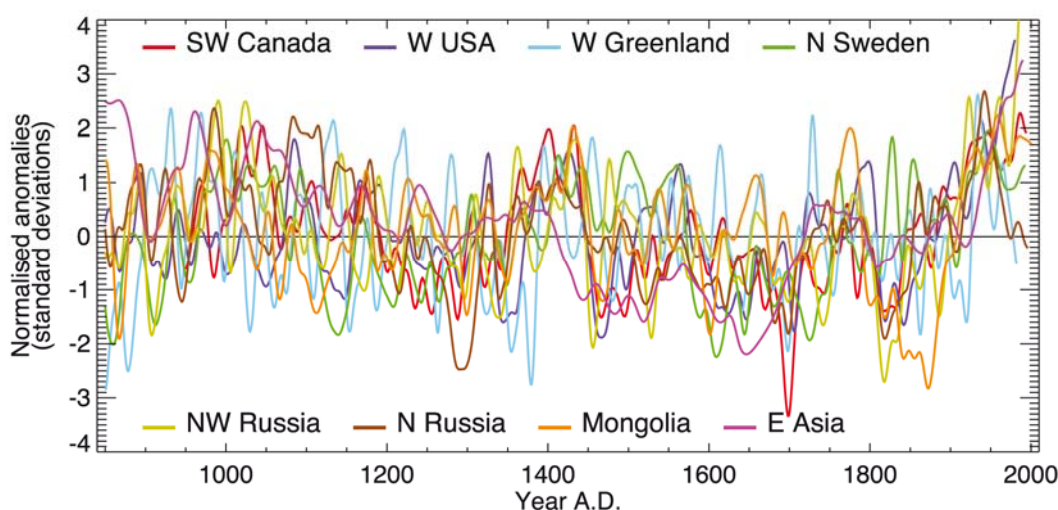


Figure 5.27. The heterogeneous nature of climate during the Medieval Warm Period is illustrated by the wide spread of values in the individual records that have been used to reconstruct the mean temperature in the Northern Hemisphere (see fig. 5.25). These records have been smoothed with a 20-year filter and scaled to have zero mean and unit standard deviation over the period 1001 to 1980. Figure 1, Box 6.4 from Jansen et al. (2007), reproduced with permission from IPCC. See Jansen et al. (2007) for a full reference to all the time series.

Analysing the sources of climate variations on a regional scale is extremely complex because some changes in the circulation can be part of the response of the climate system to the forcing. This was briefly described in section 5.5.2.1 where the tendency towards a positive NAO index in the winter following a major volcanic eruption was mentioned. It is thus very hard to disentangle the response of the circulation to the forcing from the internal variability that would be present in the absence of any forcing change. Nevertheless, a significant part of the climate variability on a regional scale in the last millennium is probably related to this internal variability, which is associated with the chaotic nature of the climate system and is thus similar to the daily changes in the weather. This can be illustrated by performing an ensemble of experiments using a climate model. For figure 5.28, five simulations have been run with exactly the same forcing but slightly different initial conditions. Because of those small differences, and of the sensitivity of the climate system to initial conditions, each simulation reproduces a different realisation of the internal variability of the modelled system (note that the observed climate also corresponds to one realisation of the internal variability of the real system among all the possibilities). While the response to the forcing is nearly identical resulting in some common characteristics for all the simulations, the large differences between the five experiments indicate that the internal variability can be the dominant source of climate changes before the 20<sup>th</sup> century.

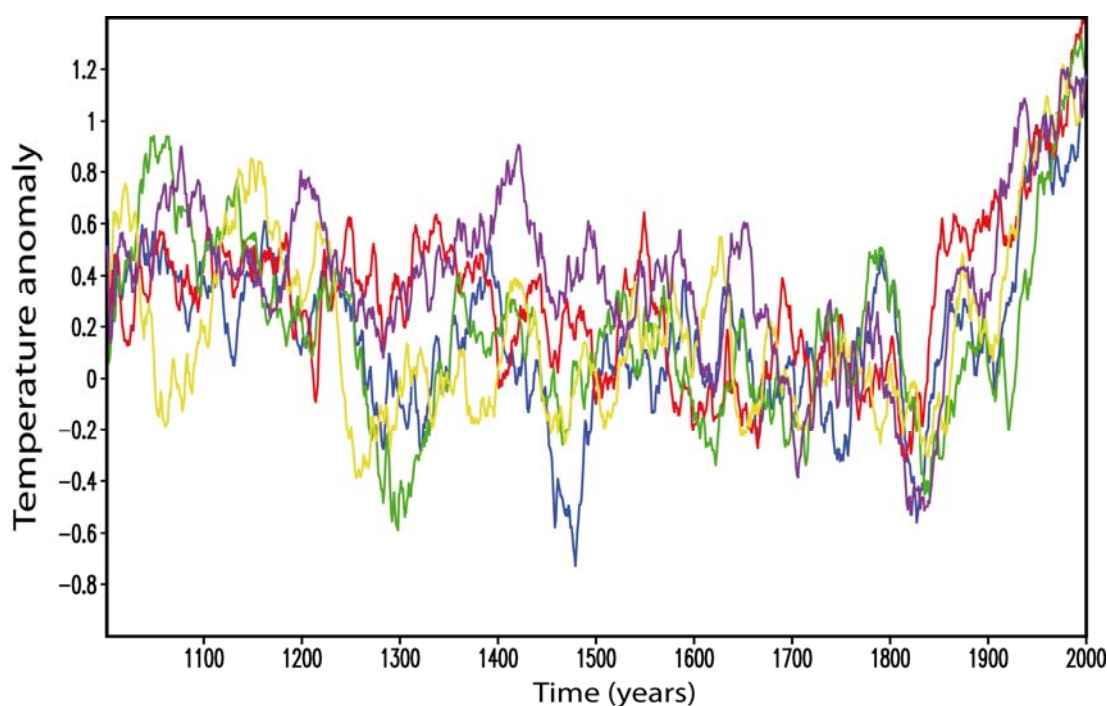


Figure 5.28. Five different simulations of the surface temperature anomaly (°C) in the Arctic (defined here as the area northward of 65°N) over the last millennium using the climate model LOVECLIM (<http://www.astr.ucl.ac.be/index.php?page=LOVECLIM%40Description>) driven by both natural and anthropogenic forcings. In the 5 experiments displayed with various colours, only the initial conditions are different resulting in a different sample of the model internal variability in each simulation. The reference period is 1601-1850 AD. Data from E. Crespin.

### 5.5.3 The last century

In the period 1906-2005, the global mean surface temperature rose by  $0.75 \pm 0.18^\circ\text{C}$  (Fig. 5.29). Moreover, the rate of warming has increased sharply, with the increase in the last 50 years being almost double that in the last 100 years. This warming, which has led to the highest temperature for at least several centuries (Fig. 5.25), is clear at global and hemispheric scale as well as over all the continents except Antarctica (Fig. 5.29). The surface temperature of the oceans is also increasing, but more slowly than that over the continents. The warming is associated with a decrease of Arctic sea ice extent, a retreat of the large majority of the glaciers, and as of the snow cover over land.

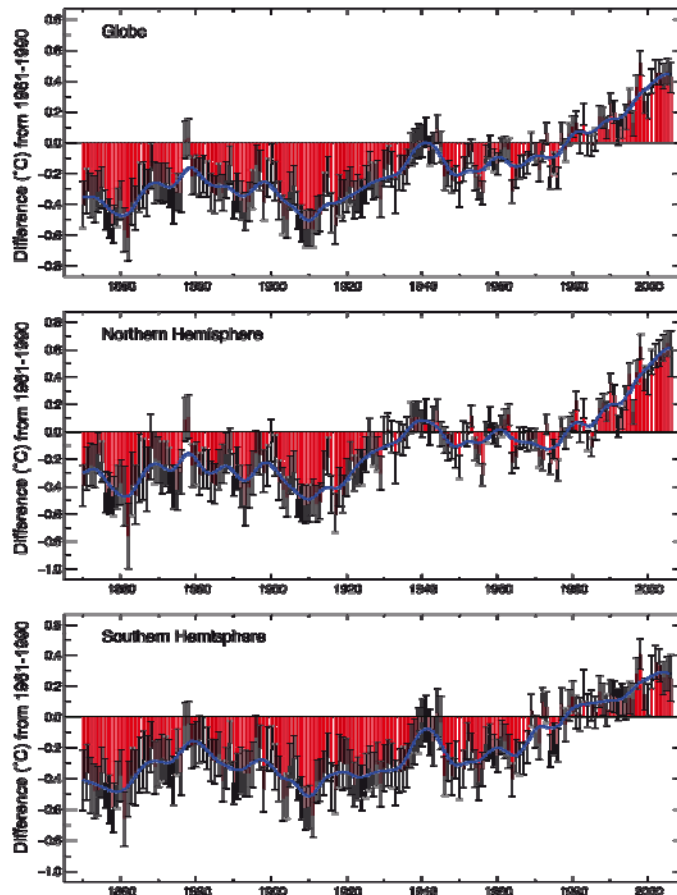


Figure 5.29 Global and hemispheric annual combined land-surface air temperature and SST anomalies ( $^\circ\text{C}$ ) (red) from 1850 to 2006 relative to the 1961 to 1990 mean, along with the 5 to 95% error bars, from HadCRUT3 (adapted from Brohan et al., 2006). The smooth blue curves show decadal variations. Figure 3.6 from Trenberth et al. (2007), reproduced with permission from IPCC.

When driven by natural forcings only, climate models cannot reproduce the observed warming. By contrast, if anthropogenic forcings are included, the results are compatible with the observed changes. The dominant anthropogenic forcing is the increase in greenhouse gas concentrations in the atmosphere. This is associated with a strong radiative forcing of about  $2 \text{ W m}^{-2}$  in 2000 compared to preindustrial conditions. Although the effect of sulphate-aerosol emission by human activities is less precisely known, one of its more robust effects is a net negative radiative forcing that partly compensates for the warming due to the greenhouse gases. Humanity has also strongly affected the land use, in particular through deforestation. This has an impact on the

chemical composition of the atmosphere, for instance when wood is burned and releases CO<sub>2</sub>. It also modifies the physical characteristics of the surface such as the **albedo**, roughness and water availability. While most of the human-induced changes in greenhouse gas concentrations and in sulphate aerosols have occurred in the last 150 years, land-use modifications started thousands of years ago in some regions, and certainly had an impact on climate at regional scale and perhaps at the global one.

The large changes in climate observed recently thus appear to be outside the range of natural variability on decadal to centennial timescales, but these changes are compatible with those predicted by models including anthropogenic forcings. This has led the IPCC to conclude, in its 4<sup>th</sup> assessment report, that: “It is very likely that anthropogenic greenhouse gas increase caused most of the observed increase in global average temperature since the mid-20<sup>th</sup> century. Without the cooling effect of atmospheric aerosols, it is likely that greenhouse gases alone would have caused a greater global mean temperature rise than observed during the last 50 years” (Solomon et al. 2007). ‘Very likely’ in this sentence means a likelihood higher than 90 %, while ‘likely’ corresponds to the 66% level. In the future, additional changes are expected, as discussed in the next chapter.

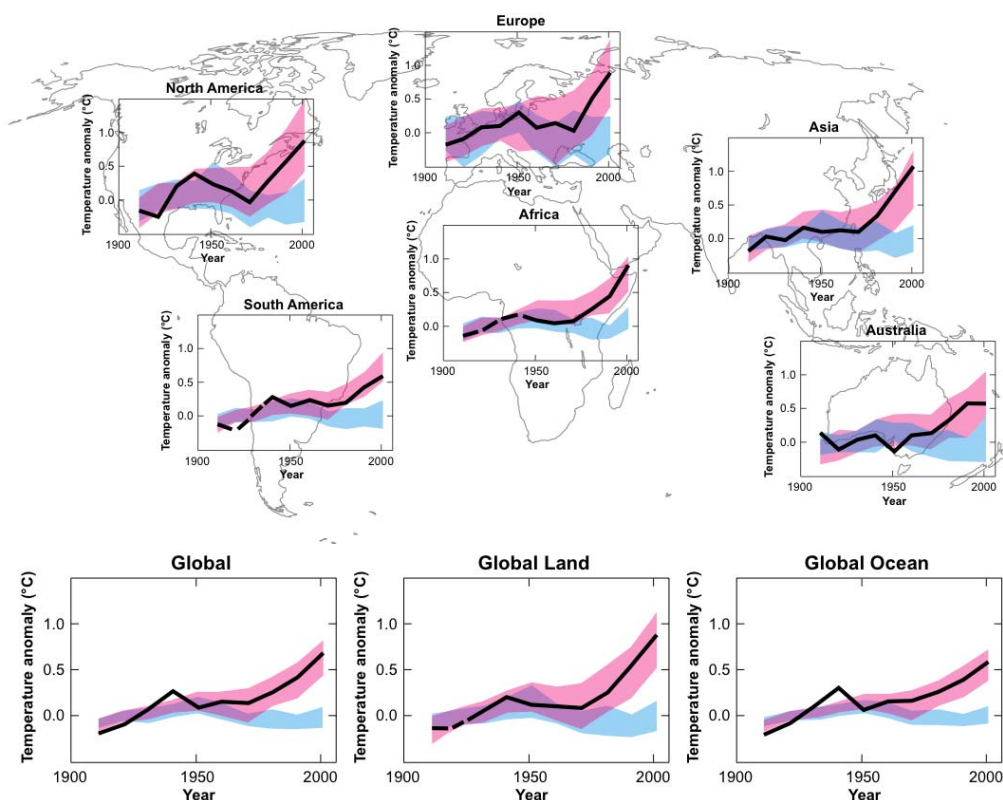


Figure 5.30 Comparison of observed continental- and global-scale changes in surface temperature with results simulated by climate models using natural and anthropogenic forcings. The decadal averages of the observations are shown for the period 1906 to 2005 (black line) plotted against the centre of the decade and relative to the corresponding average for 1901 to 1950. Lines are dashed where spatial coverage is less than 50%. Blue shaded bands show the 5% to 95% range for 19 simulations from 5 climate models using only the natural forcings due to solar activity and volcanoes. Red shaded bands show the 5% to 95% range for 58 simulations from 14 climate models using both natural and anthropogenic forcings. Figure TS22 from Solomon et al. (2007), reproduced with permission from IPCC.

## Cited references and further reading

- Berger A.L. (1978). Long-term variations of daily insolation and Quaternary climatic changes. *J. Atmos. Sci.* 35: 2363-2367
- Berger A. and M.F. Loutre (1991). Insolation values for the last 1000000 years. *Quaternary Science Reviews*, 10, 4, 297-317.
- Berger A. and M.F. Loutre (2003). Climate 400,000 years ago, a key to the future?. In : *Earth's Climate and Orbital Eccentricity. The marine isotope stage 11 question.* A.W.Droxler, R.Z.Poore, L.H.Burckle (Eds). *Geophysical Monograph* 137. AGU, Washington, DC, 17-26.
- Brohan P, J.J. Kennedy, I. Harris, S.F.B. Tett, and P.D.Jones (2006). Uncertainty estimates in regional and global observed temperature changes: A new data set from 1850. *J. Geophys. Res.* 111 (D12): Art. No. D12106.
- Committee on Abrupt Climate Change, National Research Council (2002). *Abrupt Climate Change: Inevitable Surprises* Freely available at <http://books.nap.edu/openbook.php?isbn=0309074347>
- Cuffey K.M. and G.D. Clow (1997). Temperature, accumulation, and ice sheet elevation in central Greenland through the last deglacial transition. *J. Geophys. Res.* 102, 26,383-26,396.
- Gong, D. and S. Wang (1999). Definition of Antarctic oscillation index. *Geophys. Res. Lett.* 26(4):459-462
- Hurrell, J.W., Y. Kushnir, M. Visbeck, and G. Ottersen (2003). An Overview of the North Atlantic Oscillation. *The North Atlantic Oscillation: Climate Significance and Environmental Impact*, J.W. Hurrell, Y. Kushnir, G. Ottersen, and M. Visbeck, Eds. *Geophysical Monograph Series*, 134, pp. 1-35. Available at <http://www.cgd.ucar.edu/cas/jhurrell/publications.html>
- Imbrie J., J. Hays, D.G. Martinson, A. McIntyre, A.C. Mix, J.J. Morley, N.G. Pisias, W.L. Prell, and N.J. Shackleton (1984). The orbital theory of Pleistocene climate: support from a revised chronology of the marine <sup>18</sup>O record. In: "Milankovitch and Climate", A. Berger, J. Imbrie, J. Hays, G. Kukla, B. Saltzman (eds), 269-305, D. Reidel Publ. Comp., Dordrecht, Holland.
- IPCC (2007). *Climate Change 2007: The Physical Science Basis. Contribution of Working Group I to the Fourth Assessment Report of the Intergovernmental Panel on Climate Change* [Solomon, S., D. Qin, M. Manning, Z. Chen, M. Marquis, K.B. Averyt, M.Tignor and H.L. Miller (eds.)]. Cambridge University Press, Cambridge, United Kingdom and New York, NY, USA.
- Jansen, E., J. Overpeck, K.R. Briffa, J.-C. Duplessy, F. Joos, V. Masson-Delmotte, D. Olago, B. Otto-Bliesner, W.R. Peltier, S. Rahmstorf, R. Ramesh, D. Raynaud, D. Rind, O. Solomina, R. Villalba and D. Zhang (2007). Palaeoclimate. In: *Climate Change 2007: The Physical Science Basis. Contribution of Working Group I to the Fourth Assessment Report of the Intergovernmental Panel on Climate Change* [Solomon, S., D. Qin, M. Manning, Z. Chen, M. Marquis, K.B. Averyt, M. Tignor and H.L. Miller (eds.)]. Cambridge University Press, Cambridge, United Kingdom and New York, NY, USA.



- Jones P.D. and M.E. Mann (2004). Climate over past millennia. *Rev. Geophys.* 42(2) : RG2002, DOI 10.1029/2003RG000143
- Kalnay, E. and twenty-one others (1996). The NCEP/NCAR 40-year reanalysis project. *Bull. Amer. Meteor. Soc.* 77: 437-471
- Lisiecki, L. E. and M. E. Raymo (2005). A Pliocene-Pleistocene stack of 57 globally distributed benthic  $\delta^{18}\text{O}$  records. *Paleoceanography* 20: PA1003, doi:10.1029/2004PA001071.
- Oldenborgh, G.J. van, M.A. Balmaseda, L. Ferranti, T.N. Stockdale and D.L.T. Anderson(2004). Evaluation of atmospheric fields from the ECMWF seasonal forecasts over a 15 year period. *J. Climate* 18: 2970-2989.
- Petit J.R., J. Jouzel, D. Raynaud, N.I. Barkov, J.M. Barnola, I. Basile, M. Bender, J. Chapellaz, M. Davis, G. Delaaygue, M. Delmotte, V.M. Kotlyakov, M. Legrand, V.Y. Lipenkov, C. Lorius, L. Pépin, C. Ritz, E. Saltzman., and M. Stievenard (1999). Climate and atmospheric history of the past 420,000 years from Vostok ice core, Antarctica. *Nature*, 399 (6735): 429-436.
- Rayner N.A., D.E. Parker, E.B. Horton, C.K. Folland, L.V. Alexander, D.P. Rowell, E.C. Kent and A. Kaplan (2003). Global analyses of sea surface temperature, sea ice, and nigh marine aire temperature since the late nineteenth century. *J. Geophys. Res.* 108 (D14): 4407, doi:10.1029/2002JD002670
- Ropelewski C.F., and M.S. Halpert (1987). Global and regional precipitation associated with El Niño/Southern Oscillation. *Mon. Wea. Review* 115: 1606–1626.
- Royer, D.L., R. A. Berner and J. Park (2007). Climate sensitivity constrained by CO<sub>2</sub> concentrations over the past 420 million years. *Nature* 446: 530-532.
- Solomon, S., D. Qin, M. Manning, R.B. Alley, T. Berntsen, N.L. Bindoff, Z. Chen, A. Chidthaisong, J.M. Gregory, G.C. Hegerl, M. Heimann, B. Hewitson, B.J. Hoskins, F. Joos, J. Jouzel, V. Kattsov, U. Lohmann, T. Matsuno, M. Molina, N. Nicholls, J. Overpeck, G. Raga, V. Ramaswamy, J. Ren, M. Rusticucci, R. Somerville, T.F. Stocker, P. Whetton, R.A. Wood and D. Wratt (2007). Technical Summary. In: *Climate Change 2007: The Physical Science Basis. Contribution of Working Group I to the Fourth Assessment Report of the Intergovernmental Panel on Climate Change* [Solomon, S., D. Qin, M. Manning, Z. Chen, M. Marquis, K.B. Averyt, M. Tignor and H.L. Miller (eds.)]. Cambridge University Press, Cambridge, United Kingdom and New York, NY, USA.
- Sterl A., G.J. van Oldenborgh, W. Hazeleger and G. Burgers (2007). On the robustness of ENSO teleconnections. *Climate Dynamics* 2: 469-485.
- Trenberth, K.E., P.D. Jones, P. Ambenje, R. Bojariu, D. Easterling, A. Klein Tank, D. Parker, F. Rahimzadeh, J.A. Renwick, M. Rusticucci, B. Soden and P. Zhai, 2007: Observations: Surface and Atmospheric Climate Change. In: *Climate Change 2007: The Physical Science Basis. Contribution of Working Group I to the Fourth Assessment Report of the Intergovernmental Panel on Climate Change* [Solomon, S., D. Qin, M. Manning, Z. Chen, M. Marquis, K.B. Averyt, M. Tignor and H.L. Miller (eds.)]. Cambridge University Press, Cambridge, United Kingdom and New York, NY, USA.
- Wallace, J.M. and D. S. Gutzler (1981). Teleconnections in the Geopotential Height Field during the Northern Hemisphere Winter. *Mon. Wea. Review.*109. 784-812.

Wanner H., S. Brönnimann, C. Casty, D. Gyalistras, J. Lutebacher, C. Schmutz, D.B. Stephenson and E. Xoplaki (2001). North Atlantic Oscillation – Concept and studies. *Surveys in Geophysics* 22:321-382.

Xie, P., and P. A. Arkin, 1997: Global Precipitation: A 17-Year Monthly Analysis Based on Gauge Observations, Satellite Estimates, and Numerical Model Outputs. *Bull. Amer. Meteor. Soc.* 78, 2539--2558.

Zachos J.C., G.R. Dickens and R.E. Zeebe (2008). An early Cenozoic perspective on greenhouse warming and carbon-cycle dynamics. *Nature* 451: 279-283.

## **Exercises**

Exercises are available on icampus for registered students.